HHS Public Access

Author manuscript

*Nat Neurosci*. Author manuscript; available in PMC 2015 April 01.

Published in final edited form as:

*Nat Neurosci*. 2014 October ; 17(10): 1340–1350. doi:10.1038/nn.3791.

# Activity-dependent regulation of astrocyte GAT levels during synaptogenesis

**Allie K. Muthukumar**, **Tobias Stork**, and **Marc R. Freeman**

Department of Neurobiology, University of Massachusetts Medical School, Worcester, MA 01605

Howard Hughes Medical Institute

## Abstract

Astrocytic uptake of GABA through GABA transporters (GATs) is an important mechanism regulating excitatory/inhibitory balance in the nervous system, however mechanisms by which astrocytes regulate GAT levels are undefined. Here we show at mid-pupal stages the *Drosophila* CNS neuropil is devoid of astrocyte membranes and synapses. Astrocyte membranes subsequently infiltrate the neuropil coordinate with synaptogenesis and a strocyte ablation reduces synapse numbers by half, indicating that *Drosophila* astrocytes are pro-synaptogenic. Shortly after synapses form in earnest, the GABA transporter, GAT, is up-regulated in astrocytes. Ablation or silencing of GABAergic neurons or disruption of metabotropic GABA receptor ($GABA_BR1/2$) signaling in astrocytes leads to decreased astrocytic GAT levels. Interestingly, developmental depletion of astrocytic $GABA_BR1/2$ signaling suppresses mechanosensory-induced seizure activity in mutants with hyperexcitable neurons. These data reveal astrocytes actively modulate GAT expression via metabotropic GABA receptor signaling, and highlight the importance of precise regulation of astrocytic GAT in modulation of seizure activity.

## Introduction

Brain circuits are comprised of complex ensembles of excitatory and inhibitory neurons and glial cells. Neurons and glia are intimately associated from very early developmental stages and the proper assembly of functional neural circuits is thought to require extensive neuron-glia signaling[1–6]. Defining precisely how neurons and glia communicate during development to ensure proper neural circuit assembly remains a major challenge for the field. Astrocytes have emerged as critical regulators of neuronal development, particularly with respect to promoting synapse formation [1,3,5].

Reciprocal mechanisms by which synapses might signal to astrocytes to regulate their development remain more mysterious, despite the fact that astrocytes regulate key aspects of neural circuit function, including the balance of excitatory and inhibitory neurotransmission.



*correspondence to: marc.freeman@umassmed.edu.

**Author contributions:** A.K.M. performed the experiments; T.S. generated GAT antibodies; M.R.F. supervised the project; A.K.M and M.R.F wrote the manuscript.

Glutamate is the primary excitatory neurotransmitter in the mammalian CNS and can be rapidly cleared by astrocytes via uptake through excitatory amino acid transporters (EAATs) [7,8]. The principle inhibitory neurotransmitter Gamma-aminobutyric acid (GABA) serves as a break to dampen excitatory signaling when appropriate. GABA inhibitory activity is mediated by GABA receptors (GABA-Rs) either locally at synapses where it hyperpolarizes the postsynaptic cell, or at extra-synaptic sites where it provides widespread tonic inhibition of neuronal firing[9,10]. Debilitating diseases are caused by imbalances in excitatory and inhibitory firing. For instance in epilepsy, mis-regulated GABA levels are believed to lead to hyperexcitability and ultimately seizure[11–13].

GABAergic signaling can be fine-tuned at multiple levels, including changes in GABA-R density or alterations in GABA-R subtype composition[14]. However, uptake of GABA by astrocytic GABA transporters (GATs) is also an important regulatory mechanism. GABA removal and degradation at synapses is critical for proper termination of GABAergic signaling, while uptake at non-synaptic sites can influence GABA tone across larger areas in the brain[15,16]. Reduced GAT-3 levels in mouse hippocampal astrocytes resulted in increased tonic inhibitory currents and reduced IPSC amplitudes in hippocampal interneurons, likely due to elevated GABA levels and subsequent desensitization of GABA receptors[17]. Similarly, blockade of astrocytic GAT-3 in the rat hippocampus contributes to increased extracellular GABA concentrations and increased tonic GABA receptor mediated currents in dentate granule cells[18].

Despite the importance of astrocytic GATs in modulating GABAergic signaling, surprisingly little is known about how GAT levels are established during development or dynamically regulated in the mature brain. Rat astrocytic GAT-3 immunoreactivity is detectable at birth, but does not appear to take on adult patterns of expression until postnatal week three in the cerebral cortex[19]. Interestingly, the timing of these postnatal changes coincides with periods of astrocyte morphogenesis and synaptic refinement[20]. This raises the intriguing possibility that initial GABAergic synaptic activity might contribute to shaping the spatiotemporal pattern of astrocytic GAT expression.

GABAergic signaling is also a major component of neural circuit activity in the *Drosophila* nervous system[21–23]. There is a single *Drosophila* ortholog of the mammalian GABA transporters belonging to the SLC6 family, termed GAT, which is expressed in CNS astrocytes but not neurons, suggesting that astrocytes are the primary cell type responsible for GABA clearance[23,24]. Consistent with this notion, GAT depletion from astrocytes causes profound defects in animal behavior[24].

Here we explore synapse-astrocyte interactions that underlie GAT activation and modulation in *Drosophila* astrocytes and roles for GAT in balancing excitatory and inhibitory signaling *in vivo*. We show during late metamorphosis, as the adult brain is forming, astrocyte development is tightly coupled with synaptogenesis and that *Drosophila* synapse formation depends on astrocytes. Coincident with synaptogenesis astrocytes exhibit an increase in GAT, which we show is modulated by GABAergic neuronal activity and astrocytic $GABA_BR1/2$ receptor signaling, suggesting that astrocytes regulate GAT levels by direct measurement of extracellular GABA. Finally, we demonstrate that inhibiting astrocytic

$GABA_BR1/2$ signaling strongly suppresses seizure activity in bang-sensitive mutants with hyperexcitable neurons, arguing this pathway is critical for modulating excitatory/inhibitory balance *in vivo*.

## Results

### Astrocytes invade the neuropil coordinately with synaptogenesis

During *Drosophila* metamorphosis the larval nervous system is dismantled and adult neural circuitry is constructed. The majority of pruning of larval neurites is complete by ~48 h after puparium formation (APF)[25–27]. We assayed astrocyte morphology and synapse formation in the central brain at 48, 60, 72, 84, and 96 h APF, and adult stages. Astrocyte membranes were labeled using the astrocyte driver *alrm-GAL4* with *UAS-mCD8::GFP* and co-stained for the presynaptic active zone marker Bruchpilot (nc82 antibody) to label the neuropil (Fig. 1a). We focused primarily on the antennal lobe (AL) region of the brain, which appears, based on our analysis, characteristic of astrocyte infiltration and neuropil development throughout the brain (Supplementary Fig. 1). Astrocyte cell bodies were present at the interface of the neuropil and cortex at 48 h APF, although astrocyte membranes were not observed invading the neuropil. By 60 h APF, short, thick astrocytic membrane processes infiltrated neuropil regions, and this increased significantly by 72 h APF when astrocyte processes were found throughout the neuropil. The fine branching that characterizes the bushy tufted morphology of mature astrocytes was not observed at 72 h APF (Fig. 1a, Supplementary Fig. 2). However, 84 h APF astrocytes densely infiltrated neuropil areas of the brain, and displayed fine branching and tufted morphology (Fig. 1a, Supplementary Fig. 2). A comparable morphology was observed at 96 h APF and in adults. Thus, the initial phases of astrocyte infiltration into the neuropil occurred between 60 and 84 h APF (Fig. 1a, Supplementary Fig 2).

We next sought to determine when synaptic structures were observed within the neuropil, and whether this was coordinate with astrocyte infiltration. Based on the lack of reliable postsynaptic markers for CNS synapses in *Drosophila* we turned to transmission electron microscopy (TEM) as a means to definitively identify synapses in the developing neuropil by ultrastructural criteria: we scored for the presence of a post-synaptic density in opposition to clusters of pre-synaptic vesicles, and for the presence of T-bars. We focused our analysis on the AL, mushroom body (MB), and the superior posterior slope (SPSL) neuropil regions of the brain at 48, 60, 72, 84, 96 h APF, and in the adult.

The progressive infiltration of the neuropil with astrocyte membranes coincided with the formation of morphologically identifiable synapses in the *Drosophila* pupal brain (Fig. 1b,c). At 48 h APF the neuropil was devoid of structures resembling synapses. At 60 h APF we observed the widespread appearance of immature synaptic structures, which were characterized by poorly defined post-synaptic densities that lacked pre-synaptic vesicles. By 72 h APF mature synapses were frequently observed, and continued to increase in numbers until 84 h APF, after which synaptic density and morphology remained largely unchanged. We conclude that the major wave of synaptogenesis occurs in the *Drosophila* brain between 60 and 84 h APF, and the infiltration of astrocyte membranes into the neuropil and synaptogenesis are temporally coordinated (i.e. both occur between 60 and 84 h APF).

## Astrocyte compensatory growth and requirement in the adult CNS

The above analysis raised the exciting possibility that *Drosophila* pupal astrocytes might regulate synapse formation in a manner similar to mammalian astrocytes[1,5,28]. To address this possibility, we ablated astrocytes during late metamorphosis and assayed for changes in synaptic numbers. To ablate astrocytes we used conditional expression of the pro-apoptotic gene, *head involution defective* (*hid*). Briefly, *UAS-hid* was expressed under the control of the *alrm-GAL4* driver in the presence of *tub-GAL80$^{ts}$*. GAL80$^{ts}$ is a temperature sensitive inhibitor of GAL4: at 18°C, GAL80$^{ts}$ suppresses GAL4 activity; at 25°C GAL80$^{ts}$ activity is partially inhibited allowing for low-level *Gal4/UAS* activation; and at 30°C GAL80$^{ts}$ activity is strongly inhibited and *Gal4/UAS* activation is maximal. In order to ablate astrocytes only during late metamorphosis, we reared animals at 18°C and shifted to 25°C or 30°C at ∼40 h APF and allowed animals to remain at these temperatures until eclosion (Fig. 2a).

Astrocytes were identified using anti-GAT immunofluorescence (a specific marker for astrocytes)[24] (Fig 2b). To assess the degree of ablation under each condition, cells that were positive for both anti-GAT and anti-Repo (a pan-glial nuclear marker) immunofluorescence were counted in multiple central nervous system regions including the AL, MB, subesophageal ganglion (SOG), and the abdominal segments of the thoracic ganglion (TGab), (Supplementary Fig. 3, Fig. 2b,d,e). After a shift to 25°C (moderate ablation), astrocyte numbers decreased from 22.4 ± 1.21 (n=5) to 11.8 ± 1.56 (n= 5) in the AL, from 10.2 ± 0.49 (n= 5) to 5.8 ± 0.73 (n= 5) in the MB, from 31.8 ± 1.7 (n=5) to 20.6 ± 1.9 (n= 5) in the SOG, and from 23.6 ± 1.29 (n=5) to 8.2 ± 0.73 (n= 5) in the TGab (Fig. 2d). Surprisingly, in spite of the reduction in cell numbers by ∼50% in all regions, the remaining astrocytes infiltrated the majority of the neuropil with membrane processes (Fig. 2c). Thus astrocytes exhibit significant morphological plasticity during development. Additionally, despite the significant reductions in astrocyte cell numbers in the CNS, 100% of the pupae shifted to 25°C survived to adulthood and did not display any obvious behavioral defects (Fig. 2f). This observation argues astrocytes are generated in sufficiently high numbers to accommodate significant reductions in the astrocyte population without in turn causing dramatic changes in development, animal survival, or overt behavior.

After a shift to 30°C (severe ablation) astrocyte numbers decreased more dramatically: from 24.75 ± 0.82 (n=8) to 4.5 ± 0.62 (n= 8) in the AL, from 10 ± 0.32 (n= 5) to 4.2 ± 0.58 (n= 5) in the MB, from 32.4 ± 3.04 (n=5) to 7.2 ± 1.3 (n= 5) in the SOG, and from 24.67 ± 1.7 (n=5) to 3.4 ± 0.57 (n= 7) in the TGab (Fig. 2b,e). Under these conditions, the remaining astrocyte processes appeared sparsely distributed and were unable to fully cover neuropil space (Fig. 2c). Moreover, 41% of pupae that underwent severe ablations failed to eclose, 32% died while emerging from their pupal cases, and only 27% survived as adults (Fig. 2f). The latter collection of animals were highly uncoordinated, could not walk or fly, and died within a few days (Supplementary Video 1–3). Thus, reducing the number of astrocytes in the CNS by ∼50% during synaptogenesis does not noticeably affect animal survival or overt behavior, while ablation of ∼75% or more of *Drosophila* astrocytes greatly reduces survival and results in severe defects in motor activity and ultimately death.

### *Drosophila* astrocytes are required for synaptogenesis *in vivo*

We next sought to determine whether elimination of astrocytes led to changes in synaptogenesis. Gross synapse morphology as defined above by TEM did not appear altered in astrocyte-ablated animals (Fig. 3a). Post-synaptic density (PSD) length was unchanged after astrocyte ablation (Fig. 3b) and the percentage of synapses with T-bars was unaltered (Fig. 3c). In contrast, in astrocyte ablated animals synaptic density was reduced 32% in the AL, from 37.2 ± 1.4 (n=23 sections) to 25.3 ± 0.88 (n=27 sections) synapses per 100μm$^2$; 36% in the MB, from 48.3 ± 3.8 (n=7 sections) to 30.1 ± 3.5 (n=11 sections) synapses per 100μm$^2$; 47% in the SPSL, from 30.6 ± 1.4 (n=8 sections) to 16.1 ± 3.0 (n=8 sections) synapses per 100μm$^2$ (Fig. 3b). Astrocyte ablated tissue was also marked by an increased frequency of ruptured mitochondria (Supplementary Fig. 4), which might result from a prolonged absence of astrocytes, but we are unable to definitively state whether this is a direct or indirect result of astrocyte loss.

We quantified synapse numbers at 84 h APF, the time point at which total synapse numbers reached ∼90% in control animals (Fig. 1c). We found that even at this earlier time point, synapse numbers were significantly reduced in the absence of astrocytes (Fig. 3a,d, Supplementary Fig. 4,5). Interestingly, we noticed several immature synaptic structures (similar in morphology to what was observed at 60 h APF) in astrocyte-ablated animals. Whether these structures are delayed in development and eventually mature, or fail to mature is unclear (Fig. 3a, Supplementary Fig. 6). We also examined whether neuronal architecture or survival were grossly affected in these animals. Surprisingly, gross morphology of the adult *Drosophila* brain appeared unaffected by severe astrocyte depletion. For example, after nc82 staining of the adult brain, AL glomerular organization appeared normal at the light level (Fig. 3e). Neuronal projections of second order antennal lobe projection neurons (PNs) as well as pigment dispersing factor (PDF) neurons, representing another population of higher order neurons, were morphologically normal (Fig. 3e). The number of PNs and PDF neurons were found to be comparable in control and astrocyte-ablated animals (Fig. 3f). Finally, the membranes of cortex and ensheathing glia in the adult brain exhibited normal morphology based on immunofluorescence by anti-Draper (Supplementary Fig. 7). Thus, ablation of astrocytes during late metamorphosis does not interfere in obvious ways with gross brain architecture, neurite morphology, or neuronal survival, arguing for a more direct involvement of *Drosophila* astrocytes in synapse formation.

### GAT levels are regulated by GABAergic neuron signaling

Astrocytic uptake of GABA through GATs is thought to be a key mechanism used to balance excitation and inhibition in the CNS[15,16,29]. *Drosophila* larval astrocytes express the sole *Drosophila* ortholog of the $Na^+$ and $Cl^-$ dependent GABA transporter (GAT) of the SLC6 family[23], its depletion results in uncoordinated animals that exhibit severely reduced motility in larvae and adults[24], which argues for an important role for *Drosophila* astrocytes in modulating GABA CNS tone. Intrinsic and extrinsic mechanisms that regulate how astrocytes acquire the appropriate molecular and morphological phenotypes remain poorly defined. Given that glutamatergic neuronal signaling regulates levels of the astrocyte

glutamate transporter GLT-1, and thereby astrocyte control of glutamate tone[30–33], we explored potential roles for GABAergic signaling in regulating levels of astrocytic GATs.

We first confirmed the specificity of our GAT antibody by performing Western blot analysis following knockdown of *gat* in astrocytes using *UAS-gat RNAi*. In control animals we observed a ~50 kDa band corresponding to GAT, which was eliminated in *gat* knockdown animals (Fig. 4a,b). Immunofluorescent stains using this antibody also showed robust localization of GAT to adult astrocyte membranes (Fig. 4c). GAT immunoflouresence was dramatically reduced after *gat* knockdown in astrocytes, but unchanged following *gat* knockdown in neurons (Fig. 4c, Supplementary Fig. 8). To determine the time course of GAT expression during development of the adult nervous system, we performed Western blot analysis of GAT expression in dissected pupal brains during late metamorphosis (Fig. 4d,e). Interestingly, we found that GAT levels increased during late stages of metamorphosis and displayed the most notable increase around 84 h APF, a time point at which most CNS synapses had formed (e.g. Fig. 1c). To explore the spatial relationship between astrocyte GAT proteins and GABAergic synapses we examined GAT immunostaining while labeling GABAergic presynaptic sites using the GABA neuron specific driver, *gad-GAL4*, to express *UAS-syt::eGFP*. As expected, the two markers did not co-localize but were in close association throughout the central brain (Fig. 4f).

To determine whether GABAergic neurons regulate astrocytic GAT levels, we used multiple approaches. First, we ablated GABA neurons during metamorphosis and examined GAT expression. The *gad-GAL4* driver was used to express *UAS-mCD8::mcherry* and *UAS-hid* in a conditional manner with *tub-GAL80$^{ts}$*. GABAergic neurons were ablated specifically during metamorphosis by shifting animals to 30°C (thereby activating *Gal4/UAS*) at 0 h APF (Supplementary Fig 9). Brains were then dissected and analyzed at 84 h APF. Ablation of GABA neurons was confirmed by the reduction in the number of *mCD8::mcherry* expressing cell bodies (Fig. 5a,b). The number of GABA neurons in the medial-ventral region of the brain decreased from 64.8 ± 1.2 (n = 5 brains) to 8.60 ± 2.4 (n = 5 brains) following Hid induction. Interestingly, under these conditions we observed a significant reduction in GAT expression throughout the brain by immunofluorescent stains (Fig. 5a,c). For instance, GAT levels were reduced by 33% and 37% in the AL and SOG, respectively. Quantification of astrocyte numbers revealed that ablation of GABA neurons did not result in astrocyte death (Fig. 5d), arguing against the notion that decreases in GAT were the result of astrocyte loss. CNS-wide decreases in GAT levels in GABA neuron-ablated animals were confirmed by Western blot analysis performed on 84 h APF brains (Fig. 6b,c). Finally, we found no significant change in *gat* transcripts after GABA neurons were ablated using Hid (Fig. 6d), suggesting that regulation of GAT levels by GABAergic neurons may be post-transcriptional.

We next asked whether astrocytic GAT levels were regulated by GABAergic neuronal activity using multiple genetic tools to silence or activate GABAergic neurons. Synaptic vesicle release was blocked in GABA neurons by either expressing temperature induced dominant negative Shibire (Shi$^{ts}$), or Tetanus Toxin light chain (TNT), which blocks synaptic release by cleaving Synaptobrevin. Inhibition of GABA neuron activity by Shi$^{ts}$, specifically during late metamorphosis, resulted in a 33% decrease in GAT expression (Fig.

6a,b,c). Astrocyte morphology as well as the distribution of GABA release sites appeared grossly unaffected (Supplementary Fig. 10). Similarly, expression of TNT resulted in a 33% decrease in GAT levels (Fig. 6b,c). As was the case with GABAergic neuronal ablation, *gat* mRNA levels were unchanged in response to expression of TNT in GABA neurons (Fig. 6d). We next assayed GAT expression after blocking action potential conduction by expressing the human inwardly rectifying $K^+$ channel, Kir2.1. This resulted in a 24% decrease in GAT levels (Fig. 6a,b,c). We next explored whether increased GABAergic neuronal activity could increase astrocytic GAT levels using the temperature sensitive cationic channel TrpA1 that enables temperature-induced activation of neuronal depolarization. Despite activation of TrpA1 in GABAergic neurons, we did not observe significant changes in astrocytic GAT levels (Fig. 6a,b,c).

Sensitivity of astrocyte GAT levels to GABAergic signaling could be specific to development during the major wave of CNS synaptogenesis. Alternatively, GABAergic neuronal activity might serve as a mechanism to regulate astrocyte GAT levels throughout animal life. To discriminate between these possibilities we inhibited GABA neuron activity either by blocking synaptic vesicle release with $Shi^{ts}$, or expressing Kir2.1 (using *tub-Gal80$^{ts}$*), only during adult stages. Under these conditions we did not see significant changes in GAT levels (Fig. 6e,f). This suggests that GAT expression can be fine-tuned in response to GABA release only during a specific developmental phase of neural circuit assembly (between ~60–84 h APF).

From the above data we conclude that astrocytic GAT levels are up-regulated in the CNS during the major wave of synaptogenesis, and that GAT levels in astrocytes are sensitive to GABAergic neuronal signaling during development of the adult CNS.

### Astrocyte $GABA_B$ receptors regulate GAT during development

Astrocytes are known to express a number of neurotransmitter receptors, and can be directly sensitive to neurotransmitter release[34–37]. Given our observation that synaptic release from GABAergic neurons could regulate GAT levels in astrocytes, we explored the possibility this might be regulated by GABA receptors. Astrocyte-specific knockdown of each of the *Drosophila* ionotropic GABA receptor subunits did not appear to have an effect on GAT levels (data not shown). However, knockdown of the metabotropic GABA receptor subunit *$GABA_BR2$* in astrocytes resulted in a 31% decrease in GAT expression at 84 h APF (Fig. 7a,b). $GABA_BR2$ functions through obligate dimerization with the $GABA_BR1$ subunit[38–41]. We therefore assayed the effects of $GABA_BR1$ depletion from astrocytes by RNAi and also found a 28% decrease in GAT levels (Fig. 7a,b). $GABA_BR1$ directly binds GABA while $GABA_BR2$ signals though G protein alpha o subunit ($G_{\alpha o}$) in both *Drosophila* and mammals[38,42]. Consistent with $GABA_BR2$ signaling through $G_{\alpha o}$ in astrocytes, we found that expression of *pertussis toxin* (*Ptx*), a specific enzymatic inhibitor of $G_{\alpha o}$ in *Drosophila*, resulted in a similar 30% decrease in GAT levels at 84 h APF (Fig. 7a,b). In accordance with our observation that GABAergic neuron activity-dependent regulation of astrocytic GAT was post-transcriptional, we found that inhibition of $GABA_BR1/2$ signaling via expression of *$GABA_BR2$ RNAi* or Ptx in astrocytes did not affect the amount of *gat* transcripts in the brain (Fig. 7c). Likewise, the requirement for $GABA_BR1/2$ signaling

appears limited to a developmental time window: when either $GABA_BR1$ or $GABA_BR2$ was knocked down in adult stages only there was no significant change in GAT levels (Supplementary Fig. 11, Fig. 7d,e), while developmental knockdown of $GABA_BR1$ or $GABA_BR2$ resulted in reduced GAT levels that persisted in adult animals (Fig. 7f,g). Thus, GAT expression is fine-tuned through $GABA_BR1/2$ signaling during synaptogenesis, and this developmental resetting of GAT levels ultimately determines GAT levels in the mature CNS.

### Decreasing astrocyte GAT suppresses seizure induction

A primary function for astrocytic GAT proteins is balancing excitatory and inhibitory neuronal signaling in the CNS. To explore whether decreasing astrocyte GAT levels by inhibition of the $GABA_BR1/2$ signaling pathway is sufficient to modify the balance of excitation and inhibition in the *Drosophila* CNS, we turned to behavioral studies in bang sensitive mutants, a common model used to study nervous system hyperactivity and seizure[43]. Bang sensitive mutants undergo seizure activity followed by paralysis when stimulated by mechanical shock due to neuronal hyperexcitability[44]. Intriguingly, bang sensitive mutants like *easily shocked* (*eas*)[45] are rescued from seizure activity by application of anti-epileptic drugs such as gabapentin[46] or valproate[47], both of which have been implicated in increasing extracellular GABA levels[48].

We reasoned that if impairment of astrocytic $GABA_BR1/2$ signaling could reduce functional GAT levels, GABA would not be cleared as efficiently from the CNS, and this would in turn suppress bang sensitivity in the $eas^{PC80}$ mutant background phenotype. We therefore crossed RNAi constructs targeting *$GABA_BR2$* and the *UAS-ptx* construct into the $eas^{PC80}$ mutant background, subjected animals to mechanical shock for 10 seconds to induce seizures followed by paralysis, and then assayed recovery time for 200 seconds. Consistent with previous reports, we found that while control animals recovered within 10 seconds after treatment, $eas^{PC80}$ mutants underwent robust seizure activity and paralysis with a mean recovery time of ∼77 seconds (Fig. 8a,b). Similar recovery times were observed for all driver- or UAS-alone controls in an $eas^{PC80}$ mutant background. In striking contrast, we found that $eas^{PC80}$ animals expressing astrocytic *$GABA_BR2$ RNAi* or Ptx required significantly less time (i.e. ∼43 second mean recovery time) to recover from paralysis (Fig. 8a,b). Consistent with our previous results in control animals, we found that GAT levels were reduced when $GABA_BR1/2$ signaling was inhibited in adult $eas^{PC80}$ mutant animals (Fig. 8c,d). These data provide direct functional support for the notion that $GABA_BR1/2$ signaling regulates functional GAT on astrocyte membranes in response to GABAergic neuronal activity, which is in turn important for modulation of excitation and inhibition balance in the nervous system.

## Discussion

In this study we explored the nature of astrocyte-neuron communication during assembly of the *Drosophila* adult brain. We show the major wave of synaptogenesis occurs during the second half of pupal development and that appropriate synapse formation depends on the presence of fly astrocytes. Furthermore, we find that neuronal activity can reciprocally

regulate astrocyte development. Proper up-regulation of the sole *Drosophila* GABA transporter (GAT) of the SLC6 family requires GABAergic neural activity. Astrocytes appear to sense changes in extracellular GABA through activation of metabotropic GABA receptors 1/2 ($GABA_BR1/2$). Alterations in GAT expression caused by depletion of astrocytic $GABA_BR1/2$ signaling leads to reduced GAT expression and suppression of activity-induced seizures in adult animals. Our data argue that reciprocal neuron-astrocyte signaling through $GABA_BR1/2$ is essential to balance excitatory and inhibitory firing in the adult brain.

## The formation of *Drosophila* adult CNS synapses requires astrocytes

Based on the up-regulation of selected presynaptic markers previous studies have argued that synaptogenesis occurs during late metamorphosis[25], but whether this reflected actual assembly of pre- and post-synaptic compartments and the appearance of mature synaptic structures was not known. We directly examined synapse formation by electron microscopy in multiple parts of the developing adult *Drosophila* central brain and found that the majority of synaptic structures formed between 60–84 h APF. To our knowledge, this is the first detailed ultrastructural analysis of when mature synaptic structures form in the developing adult *Drosophila* CNS. Interestingly, infiltration of astrocyte processes into the adult brain was tightly coordinated with the formation of adult brain synapses, raising the possibility that *Drosophila* astrocytes and CNS synapses might be reciprocally interdependent for formation during development. Indeed, we found genetic ablation of ~75% of an animal's astrocytes during the synaptogenic window resulted in a 30–50% (depending on brain region) reduction in synapses throughout the pupal and adult brains. This loss of synapses was accompanied by dramatic defects in adult behavior such as severe defects in motor function, although we cannot determine whether these result from deficits in synapses, astrocytes, or both.

Why was there only a partial loss of synapses in the adult when astrocytes were ablated? One possibility is that many CNS synapses in *Drosophila* may form in the absence of input from astrocytes. Astrocyte-secreted factors in mammals are critically important for both excitatory and inhibitory synapse formation *in vivo*, however no mutants affecting pro-synaptogenic astrocyte-derived molecules have been described in which more than 35% of CNS synapses are eliminated *in vivo*[3,5,49]. It also remains possible that ablation of *Drosophila* astrocytes preferentially affects specific types of synapses (e.g. cholinergic, glutamatergic, or GABAergic), which could not be determined by our EM analysis. Perhaps in the absence of astrocytes the majority of one subtype of synapse is completely eliminated. While it appears that other subtypes of *Drosophila* glia do not grow into neuropil regions and occupy the domains normally covered by astrocytes, other glial subtypes could functionally compensate for the loss of pro-synaptogenic astrocytic cues at a distance. Finally, our EM analysis was performed on the few animals that survived to adult stages, and these likely retained more astrocytes than those animals that expired at earlier developmental stages. As such, the observation that only 30–50% of synapses were eliminated could be explained by our inability to remove all astrocytes from the CNS and generate adult animals. It is possible that a small number of astrocytes can still have a pro-synaptogenic effect on their surroundings, especially since many astrocyte-secreted factors

have been shown to potently promote synapse formation. Nevertheless, our *in vivo* demonstration of a requirement for *Drosophila* astrocytes in synaptogenesis is consistent with pro-synaptogenic roles for astrocytes in mammals[1,3,5,49], and our data reveal that astrocytic control of synapse formation is a conserved feature of mammalian and invertebrate CNS development.

## Astrocyte GAT is regulated by GABAergic neuronal activity

It remains unclear how astrocytes acquire their final morphological and molecular phenotypes, and how much of this is governed by their environment. We provide mechanistic evidence for direct regulation of the astrocytic GABA transporter, GAT, in response to GABAergic neuronal activity. Western blot analysis of GAT expression during adult synaptogenesis revealed that GAT is strongly up-regulated during the major wave of synapse formation and coordinate with astrocyte infiltration of the neuropil. Strong expression of GAT is observed at 84 h APF, a developmental time point at which ~90% of synaptic structures have formed, and astrocytes have densely infiltrated neuropil regions and taken on their mature tufted morphology.

Multiple lines of evidence argue that astrocytic GAT activation is regulated directly by GABA release by GABAergic neurons. In animals at 84 h APF, ablation of GABA neurons reduced GAT levels throughout the brain. Likewise, blockade of synaptic vesicle release (using $Shi^{ts}$ and TNT) or action potential firing (using Kir2.1) in GABA neurons also resulted in reduced astrocyte GAT levels, indicating that GAT is modulated by GABA release. Interestingly, astrocytes are likely capable of directly measuring extracellular GABA levels through metabotropic GABA receptors ($GABA_BR1/2$) and adjusting GAT levels accordingly. Depletion of $GABA_BR1$ or $GABA_BR2$ by RNAi or inhibition of $G_{\alpha o}$ signaling by Ptx expression specifically in astrocytes resulted in reduced levels of GAT at late pupal stages. Somewhat surprisingly, we see this mechanism of GAT regulation to be present only during development and coincident with synaptogenesis. Adult specific manipulations of GABA neuron activity or $GABA_BR1/2$ signaling did not noticeably alter GAT expression. Nevertheless, fine tuning of GAT during development is important for establishing adult levels since knockdown of $GABA_BR1$ or $GABA_BR2$ during development reduced GAT expression even in adult stages. Direct measurement of GABA by astrocytes through $GABA_BR1/2$ signaling would provide a simple mechanism for how astrocytes adjust their levels of GAT expression (and therefore ability to clear extracellular GABA) in response to alterations in GABA release. Adult expression patterns of mammalian astrocytic GAT-3 are established during postnatal stages that also coincide with periods of neuronal circuit refinement and astrocyte maturation[19]. Furthermore, mammalian astrocytes have been found to express $GABA_B$ receptors[34,50]. We therefore speculate a similar astrocyte-synapse signaling event may therefore also modulate astrocytic GAT levels in mammals, but this awaits exploration.

Each of our manipulations resulting in block of GABAergic neural activity or $GABA_BR1/2$ signaling resulted in no more than ~50% reduction in astrocytic GAT levels. On one hand, this could be explained by the nature of the manipulations—perhaps they did not result in a complete loss of GABA neurons, neural activity or $GABA_BR1/2$ signaling. Also, because

our antibody against GAT does not distinguish between GAT that is inserted in the membrane and GAT that is retained in intracellular pools, the level of functional GAT at the membrane may in fact be less than what is observed in immunostains. Finally, it is important to note that multiple mechanisms likely exist for modulating astrocytic GAT. It is possible that the initiation of GAT expression is hardwired at some level during development to establish a baseline for handling GABA, which might explain the consistent ∼50% reduction in expression level we observed in all our manipulations of GABAergic neurons or astrocytic $GABA_B$ receptor signaling. Subsequent modulation and fine-tuning of GAT levels may then be regulated by activity-dependent plasticity imparted by $GABA_BR1/2$ signaling or other physiological mechanisms. Indeed, recent studies by Shigetomi *et al*. revealed an exciting role for astrocyte TrpA1-dependent calcium events in regulating GAT-3 levels, demonstrating another mechanism by which astrocytic GAT levels are fine-tuned. Given the significance of GABA signaling in neural circuit function, it is not surprising that multiple pathways exist to modulate GAT levels.

Modulation of GAT levels through $GABA_BR1/2$ signaling does not appear to occur at the transcriptional level. Our real-time quantitative PCR data revealed that *gat* mRNA levels are unchanged in dissected brains when GABAergic activity is blocked or when $GABA_BR1/2$ signaling is inhibited. These data argue post-transcriptional regulation is likely important for GABAergic activity-dependent changes in GAT. For example, translation of GAT mRNAs may be regulated locally, or GAT protein degradation may be regulated in response to $GABA_BR1/2$ signaling. Shigetomi *et al*. also revealed that mammalian astrocytic GAT-3 expression can be regulated by mechanisms involving dynamin-dependent endocytosis[17]. Thus, post-transcriptional regulation of astrocytic GATs may be an important manner by which astrocytes modulate GABA tone.

## Regulation of GAT in CNS excitatory/inhibitory balance

Tight regulation of GABA transporter levels and activity is critical in establishing balance between excitatory and inhibitory signaling. We provide strong behavioral evidence in the bang sensitive *Drosophila* mutant $eas^{PC80}$–a model for seizure activity[45]—that $GABA_BR1/2$ signaling can modulate extracellular GABA levels by regulating GAT expression and suppress hyperexcitability. Neurons in the $eas^{PC80}$ mutant have an altered phospholipid profile[45]. Stimulation of $eas^{PC80}$ mutant neurons by sensory input (mechanosensory) or high frequency stimulation correlates with a seizure phase, which is then followed by conduction failure and paralysis that is resolved by ∼2 minutes, whereas control animals are unaffected by these stimulations[44]. We found that inhibition of $GABA_BR1/2$ signaling by Ptx or $GABA_BR2\ RNAi$ expression in astrocytes significantly ameliorated the effects of seizure activity. These data provide *in vivo* evidence supporting a role for astrocytic $GABA_BR1/2$ signaling in modulating neural circuit function. The simplest mechanistic interpretation of our results is that inhibition of $GABA_BR1/2$ signaling results in decreased GAT, and increased levels of extracellular GABA, which in turn suppresses the effects of neuronal hyperexcitability.

Deciphering the molecular pathways mediating GAT regulation *in vivo* will be critical to understand how the balance between excitatory and inhibitory signals is maintained. Our

demonstration that $GABA_BR2$ and $G_{\alpha o}$ signaling can directly modulate GAT levels *in vivo* provides an exciting first insight into how astrocytes adjust GAT levels in response to GABA release.

## Materials and Methods

### *Drosophila* strains

The following *Drosophila* strains were used: *Canton S*, *$w^{1118}$ Canton S*, *alrm-GAL4*[51], *gad-GAL4*[52] (gift from Gero Miesenböck), *elav-GAL4*[53], *GH146-QF*[54], *UAS-mCD8::GFP*[55], *UAS-syt::eGFP*[56], *UAS-mCD8::mcherry*, *UAS-hid*[57], *UAS-shi$^{ts}$*[58], *UAS-TNT*[59] flies (active TNT-E and inactive IMPTNT-VA, gifts from John Carlson and Scott Waddell), *UAS-Kir2.1*[60], *UAS-TrpA1*[61], *UAS-ptx*[62] (gift from Vivian Budnik), *UAS-$GABA_BR1^{RNAi}$* (TRiP.JF02989), *UAS-$GABA_BR2^{RNAi}$* (VDRC transformant 1784), *UAS-$GAT^{RNAi}$* (VDRC transformant 13359), *QUAS-mCD8::GFP*[54], *tub-GAL80$^{ts}$*[63], *$eas^{PC80}$* (gift from Barry Ganetzky and Mark Tanouye).

### Temperature shift schemes

In order to assess control conditions, *GAL4* driver lines were crossed to *$w^{1118}$ Canton S* flies. For all experiments, control and experimental animals underwent identical temperature shifts. Due to variations in developmental speed at different temperatures, the following incubation periods were determined based upon assessment of morphological features corresponding to the developmental stages of interest.

**Astrocyte ablations—***alrm-GAL4* flies were crossed to *UAS-hid, tub-GAL80$^{ts}$* flies. Crosses were set up at 18°C, and 0 h APF pupae were collected and incubated at 18°C for another 48 hr. For studies conducted in the adult, the staged pupae were shifted to 25°C or 30°C until animals were one day old. For studies conducted on animals ~60 or ~84 h APF, the staged pupae were shifted to 30°C for 24 h or 48 h respectively. To assess loss of astrocytes, brains were immunostained with anti-GAT and anti-Repo antibodies. Repo positive nuclei that belonged to GAT positive cells were counted as astrocytes. When astrocytes were counted within the AL, SOG, and TGab, these neuropil regions of interest were identified by anti-HRP staining. When astrocytes were counted within the MB, anti-Fasciclin II staining was used to identify the boundaries of the MB.

**GABA neuron ablations—***gad-GAL4, UAS-mCD8::mcherry* flies were crossed to *UAS-hid, tub-GAL80$^{ts}$* flies. Crosses were raised at 18°C. Animals were collected at 0 h APF and transferred to 30°C for 72 h , at which point they displayed morphological features of 84 h APF. Loss of GABA neurons was assessed by counting the number of mcherry labeled cell bodies within a specified 100 x 110 x 50 $\mu m^3$ region in the ventral-medial region of the central brain.

**Conditional manipulation of GABA neuron activity—***gad-GAL4* flies were crossed to either *UAS-shi$^{ts}$*, *UAS-Kir2.1* with *tub-GAL80$^{ts}$*, or *UAS-trpA1* flies. Crosses were raised at 18°C, and 0 h APF pupae were collected and incubated at 18°C for another 48 h. Staged pupae were then shifted to 30°C for 48 h , at which point they displayed morphological

features of 84 h APF. For adult specific inhibition of GABA neuron activity, crosses were raised at 18°C, and 1 day old adults were shifted to 30°C for 7 days for *shi$^{ts}$* experiments and for 3 days for *Kir2.1* experiments.

## Real Time PCR

Pupal heads (84 h APF) were dissected in Jan's saline (1.8mM $Ca^{2+}$) and immediately frozen on dry ice. Total RNA was extracted using Trizol reagent. RNA pellets were resuspended in diethylpyrocarbonate (DEPC) treated water and RNA concentration was measured using a Nanodrop 2000c spectrometer (Thermo Scientific). RNA was DNase treated (DNase I, Amplification Grade, Invitrogen) and then reverse-transcribed using Superscript III First-Strand Synthesis System (Invitrogen).

Relative quantification of gene expression was performed using TaqMan probes and an ABI Prism 7000 Sequence Detection System. Platinum Quantitative PCR SuperMix-UDG w/ROX (Invitrogen) was used with the following primers and probes: gat F-primer, GGTTTGCTCCGTATCTGCTCTT; gat R-primer, GAGATTGGAAATATTCGCTGGG; gat-probe, 6FAM-TTTGGGAGCGGCGAGCTCTTCA-BHQ1; Rpl32 F-primer, GGCCCAAGATCGTGAAGAAG; Rpl32 R-primer, TAAGCTGTCGCACAAATGGC; Rpl32 probe, 6FAM-AGCACTTCATCCGCCACCAGTCG-BHQ1. Assay efficiencies were experimentally determined using a 5-point dilution series of cDNA spanning a 100-fold range in concentration (gat, 101%; Rpl32, 95%). 0.025 μg cDNA template was used per reaction. Statistical analysis was performed on $2^{-\Delta Ct}$ values.

## Immunohistochemistry

Pupal brains were dissected in PTX (0.3% Tx-100, 1XPBS) and fixed in 4% formaldehyde for 20 minutes. For adult brains and CNS preparations, heads or whole flies respectively were fixed in 4% formaldehyde for 17 minutes, washed 4 x 3 min with PTX, dissected in PTX and then fixed in 4% formaldehyde again for 7 minutes. For all preparations, the final fixation was followed by 5 quick washes with PTX and then 3 quick washes with PBT (0.1% BSA, 0.3% Tx-100, 1XPBS). Tissues were then blocked in PBT for 30 min at room temperature, and then probed with appropriate primary antibodies for 2 nights at 4°C. Samples were washed 6 x 10 minutes with PBT, probed with appropriate secondary antibodies overnight at 4°C, washed 6 x 10 minutes with PBT and then stored in Vectashield anti-fade reagent (Vector Laboratories). Antibodies were used at the following dilutions: 1:50 mouse nc82 (Developmental Studies Hybridoma Bank); 1:5000 rabbit anti-GAT; 1:10 mouse anti-PDF (Developmental Studies Hybridoma Bank); 1:500 mouse anti-GFP (Chemicon);1:150 rat anti-Fasciclin II (Developmental Studies Hybridoma Bank); 1:100 mouse anti-Elav (Developmental Studies Hybridoma Bank); 1:500 rabbit anti-Draper; 1:500 goat Cy3 conjugated anti-HRP; 1:200 donkey FITC conjugated rabbit IgG; 1:200 donkey Cy3 conjugated rabbit IgG; 1:200 donkey FITC conjugated mouse IgG; 1:200 donkey Cy3 conjugated mouse IgG (all Jackson Immunoresearch).

## Confocal microscopy

Tissues were mounted in Vectashield anti-fade reagent and imaged using a 3i Everest spinning disk confocal microscope. Whole brain images for Supplementary Fig 1 were taken

using a Zeiss EC Plan-Neofluar 10X objective (NA=0.3). Whole brain images for Fig 4f were taken using a Plan-Apochromat 20X objective. All other images were taken using a Zeiss Plan-Apochromat 40X oil objective (NA=1.3). Images were stitched together when regions of interest did not fit within the field of view (Fig. 2a).

## Immunoblotting

*Drosophila* brains were dissected in 1X PBS and collected by light centrifugation. Brains were homogenized in SDS loading buffer (60mM Tris pH 6.8, 10% glycerol, 2% SDS, 1% b-mercaptoethanol, 0.01% bromophenol blue), and centrifuged at 16000g for 10 minutes to clear the homogenate. Supernatants were then collected and boiled for 5 minutes. Samples were resolved by SDS-PAGE (BioRad), and transferred to nitrocellulose membranes (BioRad). Membranes were blocked in blocking buffer (5% Non-Fat Dry Milk, 0.01% Tween-20, 1X PBS) and then immunoblotted with appropriate antibodies. All antibodies were diluted in blocking buffer. Primary antibody incubations were performed overnight at 4°C, followed by 5 x 10 min washes in wash buffer (0.01% Tween-20, 1X PBS), appropriate HRP conjugated secondary antibody incubation for 1.5 hours at room temperature, 5 x 10 min washes in wash buffer, and then chemiluminescence detection (ECL Plus Amersham). Immunoblots were stripped by rocking in mild stripping buffer (0.2M glycine, 0.1% SDS, 1% Tween, pH 2.2) at room temperature for 10 min, followed by 2 x 5 min washes in 1XPBS, and then 2 x 5 min washes in wash buffer. After this, immunoblots were blocked again and re-probed. Antibodies were used at the following dilutions: 1:10,000 rabbit anti-GAT; 1:50,000 mouse anti-tubulin (Sigma); 1:6000 sheep HRP conjugated anti-mouse IgG (Abcam); 1:6000 goat HRP conjugated anti-rabbit IgG (Abcam).

Chemiluminescence was detected using FujiFilm Luminescent Image Analyzer LAS-4000. Western blots were analyzed using FujiFilm MultiGauge Software.

## Behavioral Assays

Flies were aged 3–7 days prior to testing. 3–10 flies were transferred to fresh food vials and vortexed for 10 seconds to provide mechanical stimulus and induce paralysis in bang sensitive animals. The numbers of flies standing and resuming normal behavior were noted at 10 s intervals until all flies had recovered from paralysis. Mean recovery time was calculated as the average time taken by an individual fly to recover from paralysis (n>100 flies for all genotypes).

## Transmission Electron Microscopy

For all EM experiments, at least two brains were independently prepared and sectioned for every condition/time-point. *Drosophila* heads were incubated in fixation buffer (2.5% glutaraldehyde in 0.1 M Sodium Cacodylate buffer pH 7.2) for 1 hour at 4°C. Brains were then dissected out in fixation buffer and incubated in fixation buffer overnight at 4°C. Samples were then processed and analyzed at the University of Massachusetts Medical School Electron Microscopy core facility according to standard procedures. Briefly, fixed samples were transferred to fresh fixation buffer and continued to incubate overnight at 4°C. Samples were rinsed 2 x with fixation buffer and treated with 1% osmium tetroxide for 1 hour at room temperature. Samples were washed 2 x with $dH_2O$ for 5 minutes and then

dehydrated through a graded ethanol series of 20% increments that ended with two changes in 100% ethanol. Samples were infiltrated with two changes of 100% propylene oxide and then with a 1:1 propylene oxide/SPI-Pon 812 resin mixture. The following day, the samples were infiltrated with 3 changes of fresh 100% SPI-Pon 812 resin, after which the samples were polymerized at 68°C in plastic capsules. Thin sections were placed on copper support grids and contrasted with lead citrate and uranyl acetate. Sections were examined using the FEI Tecani 12 BT electron microscope with 80kV accelerating voltage, and images were captured using a Gatan TEM CCD camera. The project described was supported by Award Number S10RR027897 from the National Center For Research Resources. The content is solely the responsibility of the authors and does not necessarily represent the official views of the National Center For Research Resources or the National Institutes of Health.

### Statistical Analysis

GraphPad Prism was used to perform two-tailed unpaired Student's *t*-tests, two-tailed paired Student's *t*-tests, 1-way ANOVA with Tukey's post hoc tests, and repeated measures ANOVA with Tukey's post hoc tests. Data distribution was assumed to be normal but this was not formally tested. No statistical methods were used to pre-determine sample sizes but our sample sizes are similar to those reported in previous publications. Also, data collection and analysis were not performed blind due to the conditions of the experiments. Data were not collected and processed randomly. Animals were assigned to the various experimental groups based upon genotype. A supplementary methods checklist is available.

## Supplementary Material

Refer to Web version on PubMed Central for supplementary material.

## Acknowledgments

We are grateful to Scott Waddell, Gero Miesenböck, John Carlson, Vivian Budnik, Barry Ganetsky and Mark Tanouye as well as the Vienna Drosophila RNAi Center and the Bloomington Stock Center for generously providing fly stocks. We thank the TRiP at Harvard Medical School (NIH/NIGMS R01-GM084947) for providing transgenic RNAi fly stocks and/or plasmid vectors. The antibodies nc82, anti-PDF, anti-Fasciclin II, and anti-Elav, developed by E Buchner, J Blau, C Goodman, and G.M. Rubin respectively, were obtained from the Developmental Studies Hybridoma Bank developed under the auspices of the NICHD and maintained by the University of Iowa, Department of Biological Sciences, Iowa City, IA 52242 USA. We thank the University of Massachusetts Medical School electron microscopy facility, in particular Lara Strittmatter, for expert technical assistance with EM studies. We thank Nicki Fox for critical comments on the manuscript. We thank Dwight Bergles and all members of the Freeman lab for insightful discussion on the manuscript. T.S. was supported by a postdoctoral fellowship by the Deutsche Forschungsgemeinschaft (DFG). This work was supported by NINDS grant R01NS053538 (to MRF). MRF is an Investigator with the Howard Hughes Medical Institute.

## References

1. Ullian EME, Sapperstein SKS, Christopherson KSK, Barres BAB. Control of synapse number by glia. Science. 2001; 291:657–661. [PubMed: 11158678]
2. Schafer DP, et al. Microglia sculpt postnatal neural circuits in an activity and complement-dependent manner. Neuron. 2012; 74:691–705. [PubMed: 22632727]
3. Allen NJ, et al. Astrocyte glypicans 4 and 6 promote formation of excitatory synapses via GluA1 AMPA receptors. Nature. 2012; 486:410–414. [PubMed: 22722203]
4. Eroglu C, et al. Gabapentin receptor alpha2delta-1 is a neuronal thrombospondin receptor responsible for excitatory CNS synaptogenesis. Cell. 2009; 139:380–392. [PubMed: 19818485]

5. Christopherson KS, et al. Thrombospondins are astrocyte-secreted proteins that promote CNS synaptogenesis. Cell. 2005; 120:421–433. [PubMed: 15707899]
6. Tasdemir-Yilmaz OE, Freeman MR. Astrocytes engage unique molecular programs to engulf pruned neuronal debris from distinct subsets of neurons. Genes Dev. 2014; 28:20–33. [PubMed: 24361692]
7. Su Z-Z, et al. Insights into glutamate transport regulation in human astrocytes: cloning of the promoter for excitatory amino acid transporter 2 (EAAT2). Proc. Natl. Acad. Sci. U.S.A. 2003; 100:1955–1960. [PubMed: 12578975]
8. Lehre KPK, Levy LML, Ottersen OPO, Storm-Mathisen JJ, Danbolt NCN. Differential expression of two glial glutamate transporters in the rat brain: quantitative and immunocytochemical observations. J Neurosci. 1995; 15:1835–1853. [PubMed: 7891138]
9. Isaacson JS, Solís JM, Nicoll RA. Local and diffuse synaptic actions of GABA in the hippocampus. Neuron. 1993; 10:165–175. [PubMed: 7679913]
10. Rossi DJ, Hamann M. Spillover-mediated transmission at inhibitory synapses promoted by high affinity alpha6 subunit GABA(A) receptors and glomerular geometry. Neuron. 1998; 20:783–795. [PubMed: 9581769]
11. Briggs SW, Galanopoulou AS. Altered GABA signaling in early life epilepsies. Neural Plast. 2011; 2011:527605–527605. [PubMed: 21826277]
12. Dudek FE, Staley KJ. How does the balance of excitation and inhibition shift during epileptogenesis? Epilepsy Curr. 2007; 7:86–88. [PubMed: 17520084]
13. Cope DW, et al. Enhanced tonic GABAA inhibition in typical absence epilepsy. Nat. Med. 2009; 15:1392–1398. [PubMed: 19966779]
14. Jacob TC, Moss SJ, Jurd R. GABA(A) receptor trafficking and its role in the dynamic modulation of neuronal inhibition. Nat. Rev. Neurosci. 2008; 9:331–343. [PubMed: 18382465]
15. Schousboe A. Role of Astrocytes in the Maintenance and Modulation of Glutamatergic and GABAergic Neurotransmission. Neurochem Res. 2003; 28:347–352. [PubMed: 12608708]
16. Sarup A, Larsson OM, Schousboe A. GABA transporters and GABA-transaminase as drug targets. Curr Drug Targets CNS Neurol Disord. 2003; 2:269–277. [PubMed: 12871037]
17. Shigetomi E, Tong X, Kwan KY, Corey DP, Khakh BS. TRPA1 channels regulate astrocyte resting calcium and inhibitory synapse efficacy through GAT-3. Nat. Neurosci. 2012; 15:70–80. [PubMed: 22158513]
18. Kersanté F, et al. A functional role for both GABA transporter-1 and GABA transporter-3 in the modulation of extracellular GABA and GABAergic tonic conductances in the rat hippocampus. J Physiol. 2013
19. Vitellaro-Zuccarello L, Calvaresi N. Expression of GABA transporters, GAT-1 and GAT-3, in the cerebral cortex and thalamus of the rat during postnatal development. Cell and tissue research. 2003
20. Freeman MR. Specification and morphogenesis of astrocytes. Science. 2010; 330:774–778. [PubMed: 21051628]
21. Enell LL, Hamasaka YY, Kolodziejczyk AA, Nässel DRD. gamma-Aminobutyric acid (GABA) signaling components in Drosophila: immunocytochemical localization of GABA(B) receptors in relation to the GABA(A) receptor subunit RDL and a vesicular GABA transporter. J Comp Neurol. 2007; 505:18–31. [PubMed: 17729251]
22. Küppers BB, Sánchez-Soriano NN, Letzkus JJ, Technau GMG, Prokop AA. In developing Drosophila neurones the production of gamma-amino butyric acid is tightly regulated downstream of glutamate decarboxylase translation and can be influenced by calcium. J Neurochem. 2003; 84:939–951. [PubMed: 12603819]
23. Neckameyer WS, Cooper RL. GABA transporters in Drosophila melanogaster: molecular cloning, behavior, and physiology. Invert Neurosci. 1998; 3:279–294. [PubMed: 10212397]
24. Stork T, Sheehan A, Tasdemir-Yilmaz OE, Freeman MR. Neuron-Glia Interactions through the Heartless FGF Receptor Signaling Pathway Mediate Morphogenesis of Drosophila Astrocytes. Neuron. 2014; 83:388–403. [PubMed: 25033182]
25. Jefferis GSXEG, et al. Developmental origin of wiring specificity in the olfactory system of Drosophila. Development. 2004; 131:117–130. [PubMed: 14645123]

26. Marin EC, Watts RJ, Tanaka NK, Ito K, Luo L. Developmentally programmed remodeling of the Drosophila olfactory circuit. Development. 2005; 132:725–737. [PubMed: 15659487]
27. Zhu S, Chiang A-S, Lee T. Development of the Drosophila mushroom bodies: elaboration, remodeling and spatial organization of dendrites in the calyx. Development. 2003; 130:2603–2610. [PubMed: 12736205]
28. Hughes EG, Elmariah SB, Balice-Gordon RJ. Astrocyte secreted proteins selectively increase hippocampal GABAergic axon length, branching, and synaptogenesis. Molecular and Cellular Neuroscience. 2010; 43:136–145. [PubMed: 19850128]
29. Madsen KK, White HS, Schousboe A. Neuronal and non-neuronal GABA transporters as targets for antiepileptic drugs. Pharmacol. Ther. 2010; 125:394–401. [PubMed: 20026354]
30. Benediktsson AM, et al. Neuronal activity regulates glutamate transporter dynamics in developing astrocytes. Glia. 2012; 60:175–188. [PubMed: 22052455]
31. Tanaka K, et al. Epilepsy and exacerbation of brain injury in mice lacking the glutamate transporter GLT-1. Science. 1997; 276:1699–1702. [PubMed: 9180080]
32. Devaraju P, Sun M-Y, Myers TL, Lauderdale K, Fiacco TA. Astrocytic group I mGluR dependent potentiation of astrocytic glutamate and potassium uptake. J. Neurophysiol. 2013
33. Yang Y, et al. Presynaptic regulation of astroglial excitatory neurotransmitter transporter GLT1. Neuron. 2009; 61:880–894. [PubMed: 19323997]
34. Charles KJ, Calver AR, Jourdain S, Pangalos MN. Distribution of a GABAB-like receptor protein in the rat central nervous system. Brain Res. 2003; 989:135–146. [PubMed: 14556935]
35. Uwechue NM, Marx M-C, Chevy Q, Billups B. Activation of glutamate transport evokes rapid glutamine release from perisynaptic astrocytes. J Physiol. 2012
36. Porter JT, McCarthy KD. Astrocytic neurotransmitter receptors in situ and in vivo. Prog. Neurobiol. 1997; 51:439–455. [PubMed: 9106901]
37. Hamilton NB, Attwell D. Do astrocytes really exocytose neurotransmitters? Nat. Rev. Neurosci. 2010; 11:227–238. [PubMed: 20300101]
38. Padgett CL, Slesinger PA. GABAB receptor coupling to G-proteins and ion channels. Adv. Pharmacol. 2010; 58:123–147. [PubMed: 20655481]
39. Mezler M, Müller T, Raming K. Cloning and functional expression of GABA(B) receptors from Drosophila. Eur J Neurosci. 2001; 13:477–486. [PubMed: 11168554]
40. Bettler BB, Kaupmann KK, Mosbacher JJ, Gassmann MM. Molecular structure and physiological functions of GABA(B) receptors. Physiol Rev. 2004; 84:835–867. [PubMed: 15269338]
41. Kaupmann K, et al. GABA(B)-receptor subtypes assemble into functional heteromeric complexes. Nature. 1998; 396:683–687. [PubMed: 9872317]
42. Dahdal D, Reeves DC, Ruben M, Akabas MH, Blau J. Drosophila pacemaker neurons require g protein signaling and GABAergic inputs to generate twenty-four hour behavioral rhythms. Neuron. 2010; 68:964–977. [PubMed: 21145008]
43. Parker L, Howlett IC, Rusan ZM, Tanouye MA. Seizure and epilepsy: studies of seizure disorders in Drosophila. Int. Rev. Neurobiol. 2011; 99:1–21. [PubMed: 21906534]
44. Pavlidis P, Tanouye MA. Seizures and failures in the giant fiber pathway of Drosophila bang-sensitive paralytic mutants. J Neurosci. 1995; 15:5810–5819. [PubMed: 7643221]
45. Pavlidis P, Ramaswami M, Tanouye MA. The Drosophila easily shocked gene: a mutation in a phospholipid synthetic pathway causes seizure, neuronal failure, and paralysis. Cell. 1994; 79:23–33. [PubMed: 7923374]
46. Reynolds ER, et al. Treatment with the antiepileptic drugs phenytoin and gabapentin ameliorates seizure and paralysis of Drosophila bang-sensitive mutants. J Neurobiol. 2004; 58:503–513. [PubMed: 14978727]
47. Kuebler D, Tanouye M. Anticonvulsant valproate reduces seizure-susceptibility in mutant Drosophila. Brain Res. 2002; 958:36–42. [PubMed: 12468028]
48. Sills GJ, Brodie MJ. Update on the mechanisms of action of antiepileptic drugs. Epileptic Disord. 2001; 3:165–172. [PubMed: 11844711]
49. Kucukdereli H, et al. Control of excitatory CNS synaptogenesis by astrocyte-secreted proteins Hevin and SPARC. Proc. Natl. Acad. Sci. U.S.A. 2011; 108:E440–E449. [PubMed: 21788491]

50. Oka M, Wada M, Wu Q, Yamamoto A, Fujita T. Functional expression of metabotropic GABAB receptors in primary cultures of astrocytes from rat cerebral cortex. Biochem. Biophys. Res. Commun. 2006; 341:874–881. [PubMed: 16455058]
51. Doherty J, Logan MA, Taşdemir OE, Freeman MR. Ensheathing glia function as phagocytes in the adult Drosophila brain. J Neurosci. 2009; 29:4768–4781. [PubMed: 19369546]
52. Ng M, et al. Transmission of olfactory information between three populations of neurons in the antennal lobe of the fly. Neuron. 2002; 36:463–474. [PubMed: 12408848]
53. Luo L, Liao YJ, Jan LY, Jan YN. Distinct morphogenetic functions of similar small GTPases: Drosophila Drac1 is involved in axonal outgrowth and myoblast fusion. Genes Dev. 1994; 8:1787–1802. [PubMed: 7958857]
54. Potter CJ, Tasic B, Russler EV, Liang L, Luo L. The Q system: a repressible binary system for transgene expression, lineage tracing, and mosaic analysis. Cell. 2010; 141:536–548. [PubMed: 20434990]
55. Lee T, Lee A, Luo L. Development of the Drosophila mushroom bodies: sequential generation of three distinct types of neurons from a neuroblast. Development. 1999; 126:4065–4076. [PubMed: 10457015]
56. Zhang YQ, Rodesch CK, Broadie K. Living synaptic vesicle marker: synaptotagmin-GFP. Genesis. 2002; 34:142–145. [PubMed: 12324970]
57. Grether ME, Abrams JM, Agapite J, White K, Steller H. The head involution defective gene of Drosophila melanogaster functions in programmed cell death. Genes Dev. 1995; 9:1694–1708. [PubMed: 7622034]
58. Kitamoto T. Conditional modification of behavior in Drosophila by targeted expression of a temperature–sensitive shibire allele in defined neurons. J Neurobiol. 2001
59. Sweeney ST, Broadie K, Keane J, Niemann H, O'Kane CJ. Targeted expression of tetanus toxin light chain in Drosophila specifically eliminates synaptic transmission and causes behavioral defects. Neuron. 1995; 14:341–351. [PubMed: 7857643]
60. Baines RA, Uhler JP, Thompson A, Sweeney ST, Bate M. Altered electrical properties in Drosophila neurons developing without synaptic transmission. J Neurosci. 2001; 21:1523–1531. [PubMed: 11222642]
61. Hamada FN, et al. An internal thermal sensor controlling temperature preference in Drosophila. Nature. 2008; 454:217–220. [PubMed: 18548007]
62. Ferris J, Ge H, Liu L, Roman G. G(o) signaling is required for Drosophila associative learning. Nat. Neurosci. 2006; 9:1036–1040. [PubMed: 16845387]
63. McGuire SE, Le PT, Osborn AJ, Matsumoto K, Davis RL. Spatiotemporal rescue of memory dysfunction in Drosophila. Science. 2003; 302:1765–1768. [PubMed: 14657498]

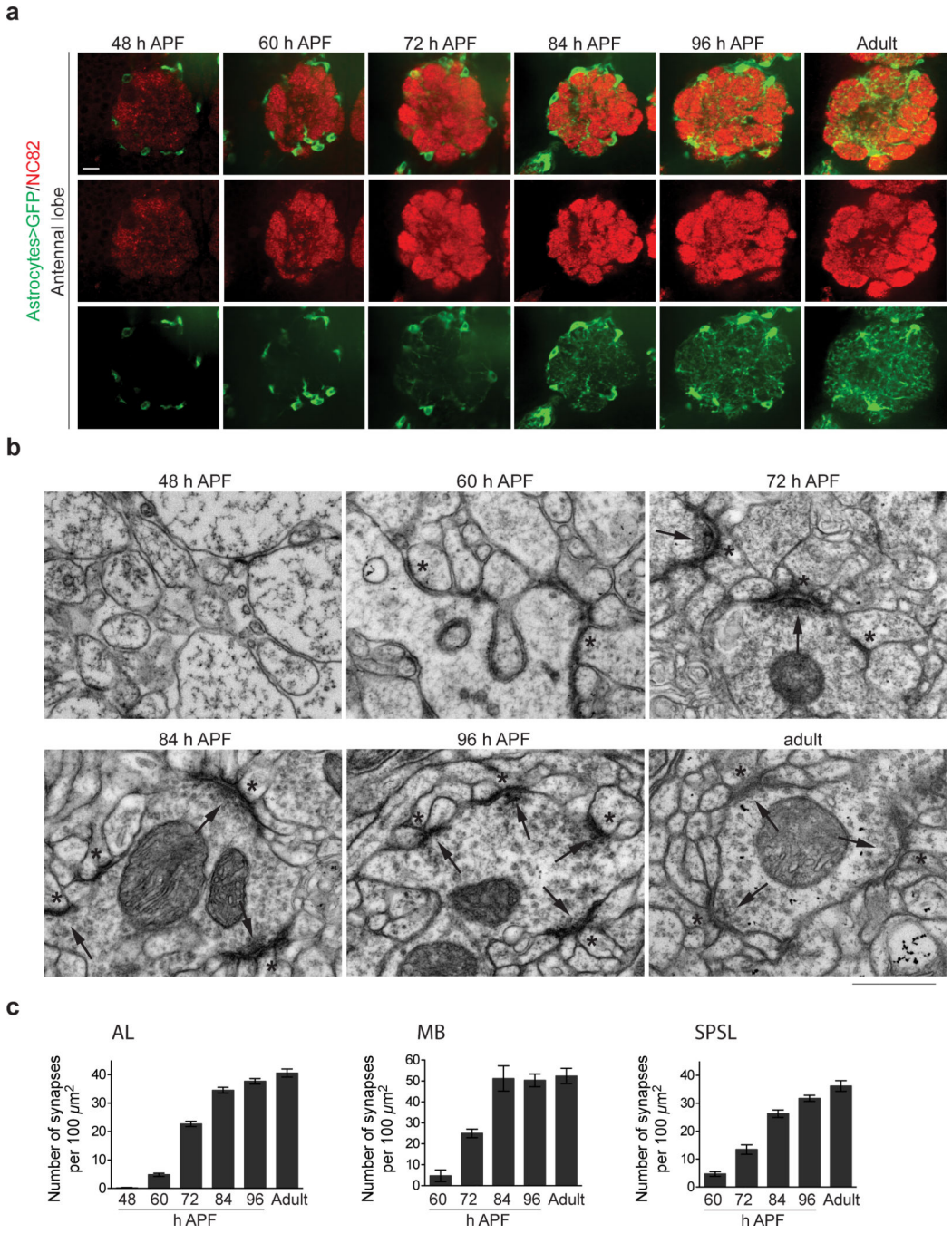


**Figure 1. Astrocyte infiltration and synaptogenesis are temporally correlated during late metamorphosis**

**(a)** Confocal section through the AL region showing astrocyte infiltration at several timepoints during metamorphosis. Astrocyte membranes are labeled by *UAS-mCD8::GFP* expression using the *alrm-GAL4* driver (green), and neuropil is labeled by nc82 antibody staining (red). Scale bar = 10μm. **(b)** Ultrastructure of AL neuropil at several timepoints during metamorphosis, highlighting the progression in synapse development. Arrows point to pre-synaptic sites and asterisks mark post-synaptic structures. Synaptic structures are

prominent starting at 72 h APF. Scale bar = 0.5μm. **(c)** Quantification of the number of synaptic structures in the AL (n ≥ 20 sections for each timepoint), MB (n ≥ 6 sections for each timepoint), and SPSL (n ≥ 9 sections for each timepoint) during late metamorphosis. Error bars, s.e.m.

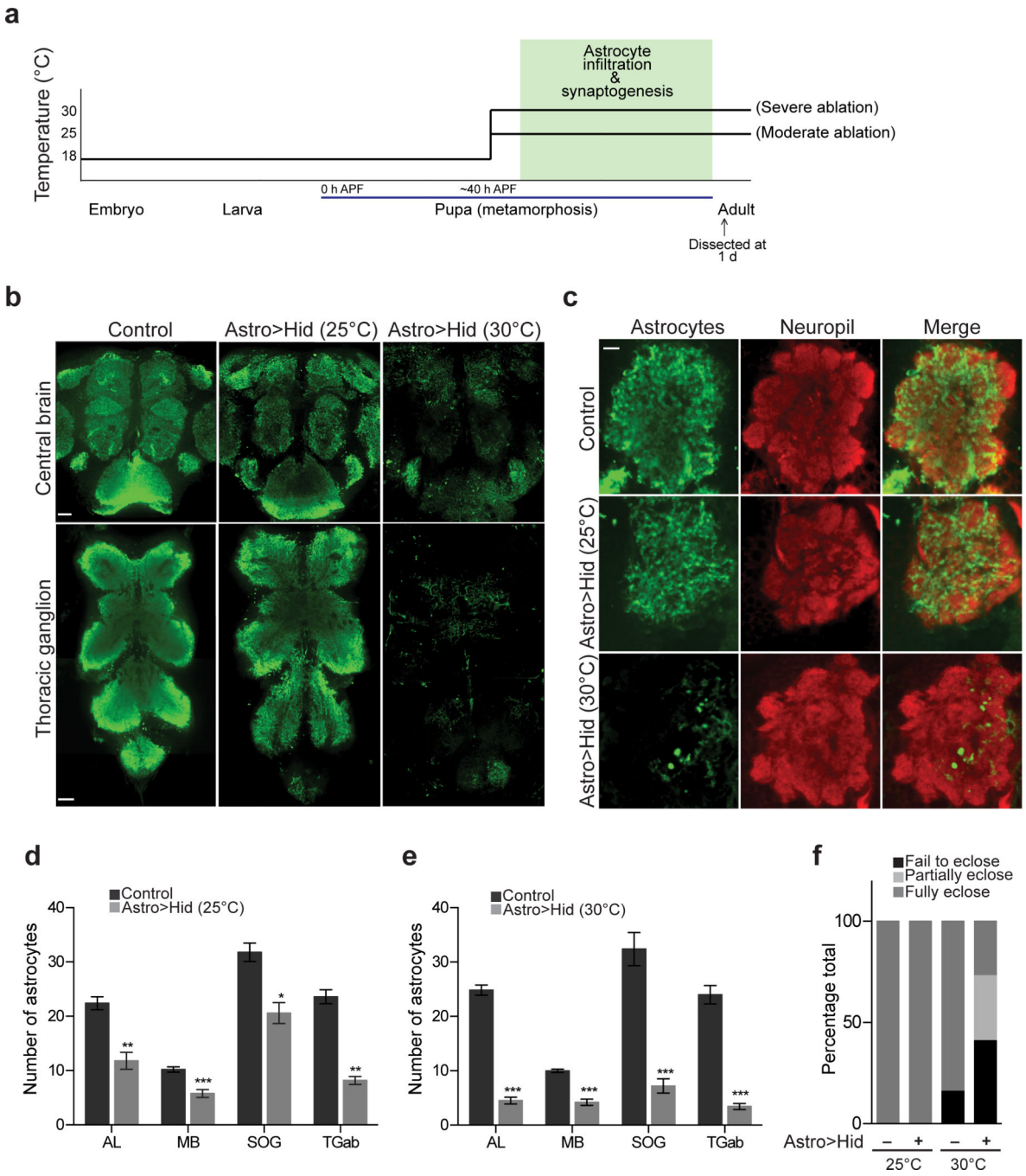


**Figure 2. Genetic ablation of astrocytes during synaptogenesis**

**(a)** Temperature shift scheme for astrocyte ablations. The *alrm-GAL4* driver and *tub-GAL80$^{ts}$* were used to conditionally express *UAS-hid* in astrocytes specifically during late metamorphosis. Varying degrees of GAL80 activity and UAS-*hid* expression were achieved by varying the incubation temperature during late metamorphosis. Low-level Hid expression was achieved at 25°C and maximal Hid expression was achieved at 30°C. **(b)** Confocal slice of central brain and ventral nerve cord of adult animals immunostained with anti-GAT antibody to visualize astrocytes. Astrocyte staining is moderately reduced following Hid

expression in astrocytes at 25°C, and robustly reduced after Hid expression in astrocytes at 30°C, indicating moderate and severe ablation conditions, respectively. Scale bar = 10μm. **(c)** Confocal sections through AL of adult animals where astrocytes are labeled by anti-GAT antibody staining (green) and neuropil is labeled by anti-HRP antibody staining (red). Astrocyte processes can fully cover neuropil space when ablations are performed at 25°C. Large regions of neuropil are left unoccupied by astrocyte processes when ablations are performed at 30°C. Scale bar = 10μm. **(d)** Number of astrocytes remaining in the AL, MB, SOG, and TGab of the adult CNS following moderate (25°C) astrocyte ablations (n = 5 brains for control and >Astro>Hid AL, MB, SOG, and TGab). **(e)** Number of astrocytes remaining in the AL, MB, SOG, and TGab of the adult CNS following severe (30°C) astrocyte ablations (n = 7 brains, control AL; n = 8 brains, >Astro>Hid AL; n = 5 brains, control and >Astro>Hid MB; n = 5 brains, control and >Astro>Hid SOG; n = 5 brains, control TGab; n = 7 brains, >Astro>Hid TGab). Fewer astrocytes remain when ablations are performed at 30°C, compared to 25°C; demonstrating the varying degrees of astrocyte ablation achieved by the two temperature conditions. **(f)** Fates of animals undergoing ablation procedure (n ≥ 30 flies for each condition). The majority of animals struggle to eclose when undergoing severe astrocyte ablations (30°C). *P≤0.05, **P≤0.01, ***P≤0.001, unpaired Student’s t-test. Error bars, s.e.m.

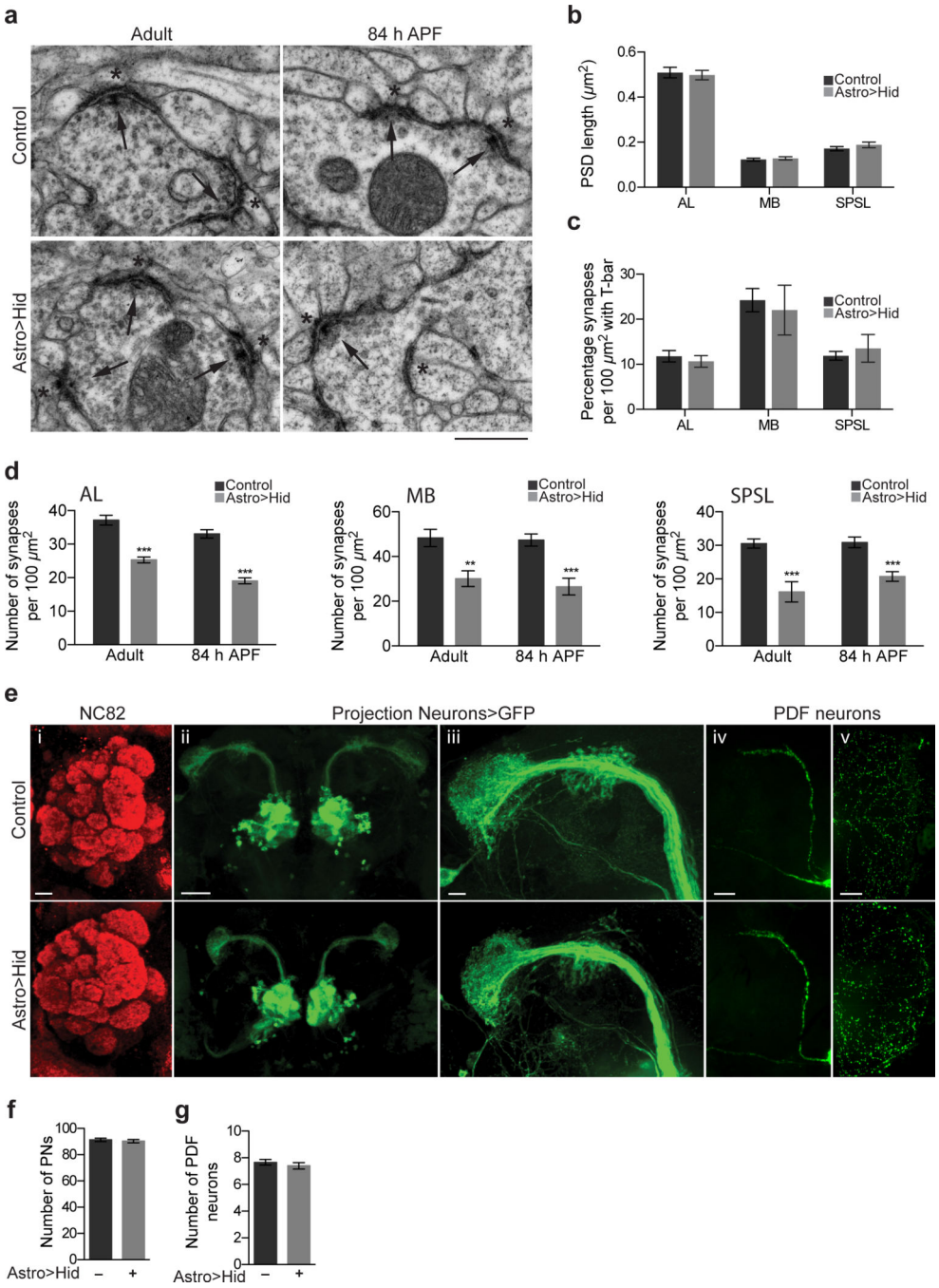


**Figure 3. Synapse number, but not gross neural architecture, is altered when astrocytes are ablated during late metamorphosis**

**(a)** Ultrastructure of synapses in the AL at adult and 84 h APF animals following 30°C astrocyte ablation. Morphology of mature synaptic structures is unaltered by ablation. Arrows point to pre-synaptic sites and asterisks mark post-synaptic structures. Scale bar = 0.5μm. **(b)** Quantification of post-synaptic density (PSD) length in AL, MB, and SPSL regions of the adult brain after 30°C astrocyte ablation (n = 80 PSDs from 12 sections, AL control; n = 81 PSDs from 12 sections, AL Astro>Hid; n = 47 PSDs from 7 sections, MB

control; n = 50 PSDs from 7 sections, MB Astro>Hid; n = 58 PSDs from 7 sections, SPSL control; n = 63 PSDs from 7 sections, SPSL Astro>Hid. **(c)** Quantification of the percentage of synapses with T-bar morphology in the AL, MB, and SPSL regions of the adult brain after 30°C astrocyte ablation (n = 23 sections, AL control; n = 24 sections, AL Astro>Hid; n = 7 sections, MB control; n = 11 sections, MB Astro>Hid; n = 8 sections, SPSL control; n = 8 sections, SPSL Astro>Hid. **(d)** Quantification of the number of synaptic structures in the AL, MB, and SPSL regions of adult and 84 h APF animals following 30°C astrocyte ablation (n = 17 sections, AL adult control; n = 22 sections, AL adult Astro>>Hid; n = 19 sections, AL 84 h APF control; n = 20 sections, AL 84 h APF >Astro>Hid; n = 17 sections, MB adult control; n = 22 sections, MB adult Astro>>Hid; n = 19 sections, MB 84 h APF control; n = 20 sections, MB 84 h APF >Astro>Hid; n = 17 sections, SPSL adult control; n = 22 sections, SPSL adult Astro>>Hid; n = 19 sections, SPSL 84 h APF control; n = 20 sections, SPSL 84 h APF Astro>>Hid. **(e)** Brain architecture is grossly unaltered following astrocyte ablations performed at 30°C. Projected confocal z-stacks showing (i) glomeruli structure in brains stained with nc82 antibody (red), (ii) morphology of PNs marked by *GH146-QF/QUAS-mCD8::GFP*, (iii) morphology of axonal projections and arborizations of PNs, (iv) morphology of PDF neuron axonal projections in the central brain, (v) morphology of PDF neuron dendritic arborizations in the optic lobe. Scale bar = 10μm for (i) and (iii); 50μm for (ii); 25μm for (iv) and (v). **(f)** Quantification of the number of PNs per hemisphere (n = 6 brains, control and Astro>>Hid) and **(g)** $PDF^+$ neurons per hemisphere (n = 6 brains, control; n = 5 brains, Astro>>Hid) following 30°C astrocyte ablation. ***P≤0.001, unpaired Student's t-test for (b–d), and (f–g). Error bars, s.e.m.

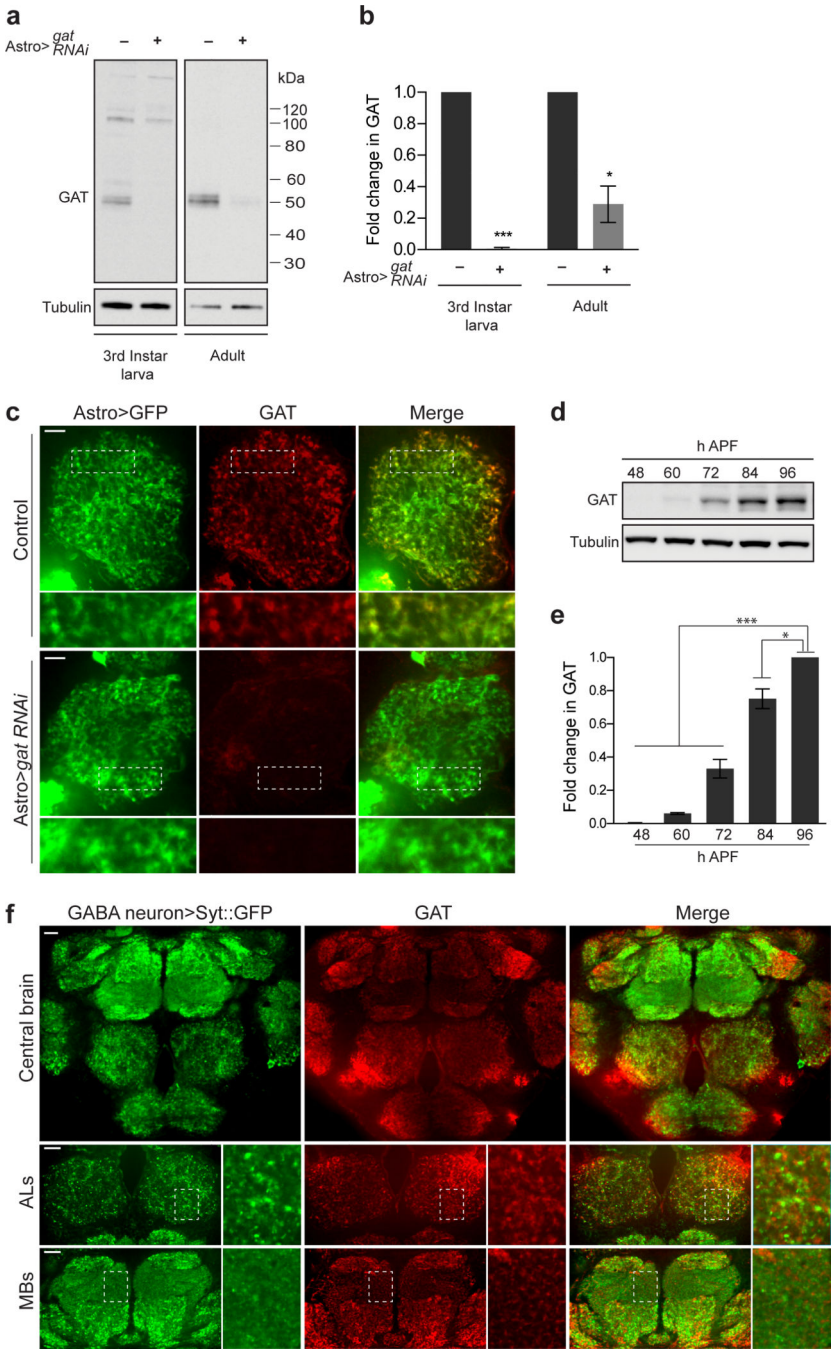


**Figure 4. GAT is exclusively expressed in astrocytes and activated during synaptogenesis**

**(a)** *UAS-gat RNAi* was expressed in astrocytes using the *alrm-GAL4* driver. Western blots performed on larval CNS and adult brain lysates were probed with anti-GAT antibody to confirm specific knockdown of GAT in astrocytes. GAT runs at approximately 50kDa. (**b**) Quantification of GAT levels from Western blot analysis shown in (a) (n = 3 experiments, 3rd instar larva; n = 3 experiments, adult).

**(c)** The *alrm-GAL4* driver was used to co-express *UAS-mCD8::GFP* and *UAS-gat RNAi*, or express *UAS-mCD8::GFP* alone. Adult brains were stained with anti-GAT antibody.

Confocal section through AL shows that GAT (red) localizes specifically to astrocyte membranes (green). Scale bar = 10μm. **(d)** Western blot performed on WT brain lysates from several stages of metamorphosis was probed with anti-GAT antibody. (**e**) Quantification of GAT levels from Western blot analysis shown in (d) (n = 3 experiments). (**f**) Adult brains expressing *UAS-syt::eGFP* using the *gad-GAL4* driver were stained with anti-GAT antibody. GABAergic pre-synaptic sites (GABA neuron>Syt::eGFP) and GAT protein are present through out the central brain. High magnification images of the AL and MB regions show that GABAergic pre-synaptic sites and GAT proteins are in close association. Scale bar = 20μm. *P≤0.05, ***P≤0.001, unpaired Student's t-test for (b) and 1-way ANOVA with Tukey's post hoc test for (e). Error bars, s.e.m. Full-length blots are presented in Supplementary Fig. 12.

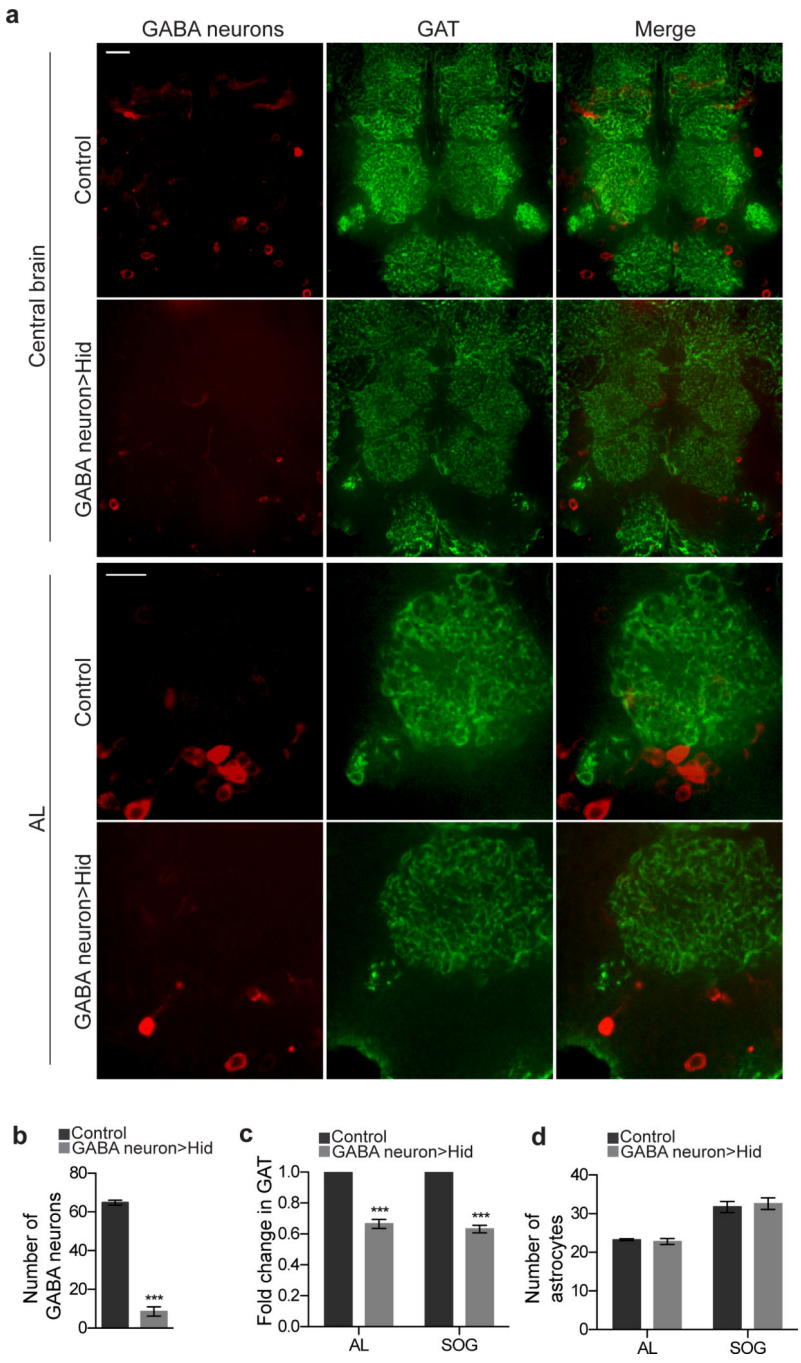


**Figure 5. GAT expression is sensitive to GABA neurons**

**(a)** Confocal sections showing anti-GAT immunostaining (green) in the central brain and AL region after ablation of GABA neurons. GABA neurons are labeled by UAS-mCD8::mcherry expression using the *gad-GAL4 driver* (red). Significant reduction in GAT levels is seen throughout the central brain in correspondence with a reduction in GABA neurons. Localization of GAT appears unaltered by GABA neuron ablations, as highlighted in images from the AL. Animals were 84 h APF upon preparation. Scale bar = 20μm. **(b)** Quantification of the number of GABA neurons in the ventral medial region of the central

brain (n = 5 brains for control and GABA neuron>>Hid). **(c)** Quantification of the mean GAT intensity in the AL and SOG regions (n = 8 brains for control and GABA neuron>>Hid for AL and SOG). **(d)** Quantification of the number of astrocytes in the AL and SOG regions (n = 4 brains, control AL; n = 5 brains, GABA neuron>>Hid AL, n = 4 brains, control SOG; n = 5 brains, GABA neuron>>Hid SOG). ***P≤0.001, unpaired Student's t-test for (b) and (d), paired Student's t-test for (c). Error bars, s.e.m.

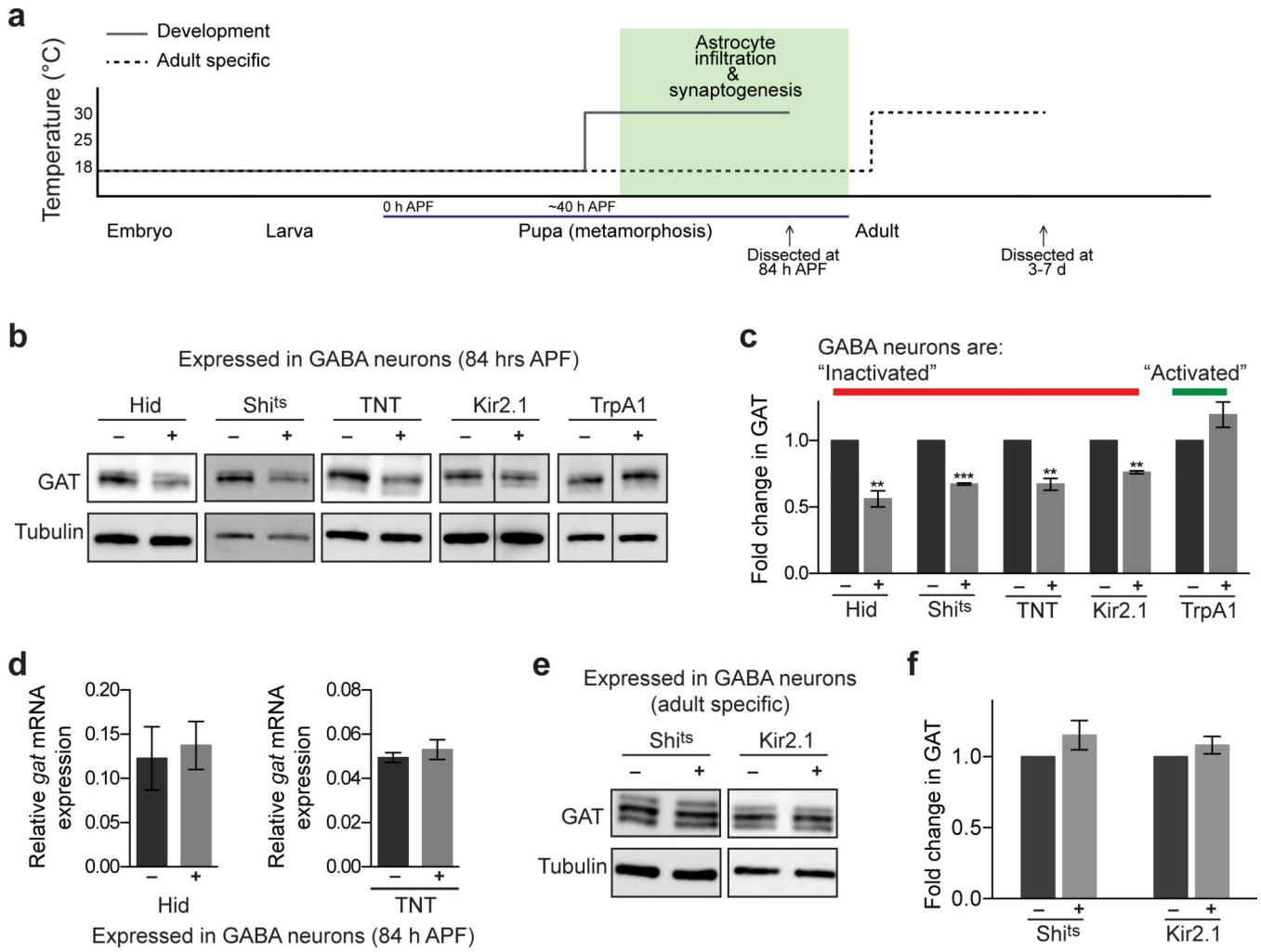


**Figure 6. GAT expression is fine tuned in response to GABA release specifically during synaptogenesis**

**(a)** Temperature shift scheme for conditional manipulation of GABA neuron activity. The temperature sensitive constructs, *UAS-shi*$^{ts}$ and *UAS-trpA1*, as well as *UAS-Kir2.1* with *tub-GAL80*$^{ts}$, were activated in a conditional manner using the *gad-GAL4* driver. Dominant negative *shi*$^{ts}$ expression, Kir2.1 expression, or TrpA1 activation was induced at 30°C. **(b)** Western blots performed on brains 84 h APF following various neuronal manipulations using the *gad-GAL4* driver. Blots were probed with anti-GAT antibody. GABA neurons were "inactivated" with expression of *UAS-hid UAS-shi*$^{ts}$ *UAS-TNT*, and *UAS-Kir2.1*. Alternatively, GABA neurons were "activated" using *UAS-trpA1***(c)** Quantification of GAT levels from Western blot analysis shown in (b) (n = 4 experiments, Hid; n = 3 experiments, Shi$^{ts}$; n = 5 experiments, TNT; n = 3 experiments, Kir2.1; n = 3 experiments, TrpA1). GAT levels are significantly reduced when GABA neurons are "inactivated." This is in contrast to unaltered GAT levels when GABA neurons are "activated." **(d)** Relative *gat* mRNA levels are unaltered when GABA neuronal activity is silenced by expression of *UAS-hid* (n = 3) or *UAS-TNT* (n = 3) using the *gad-GAL4* driver. **(e)** Western blots performed on adult brains following adult specific silencing of GABA neuronal activity by expression of *UAS-shi*$^{ts}$ or

*UAS-kir2.1* using the *gad-GAL4* driver. **(f)** Quantification of GAT levels from Western blot analysis shown in (e) (n = 3 experiments, $Shi^{ts}$; n = 3 experiments, Kir2.1). **P≤0.01, ***P≤0.001, paired Student's t-test for (c) and (f), unpaired Student's t-test for (d). Error bars, s.e.m. Full-length blots are presented in Supplementary Fig. 12.

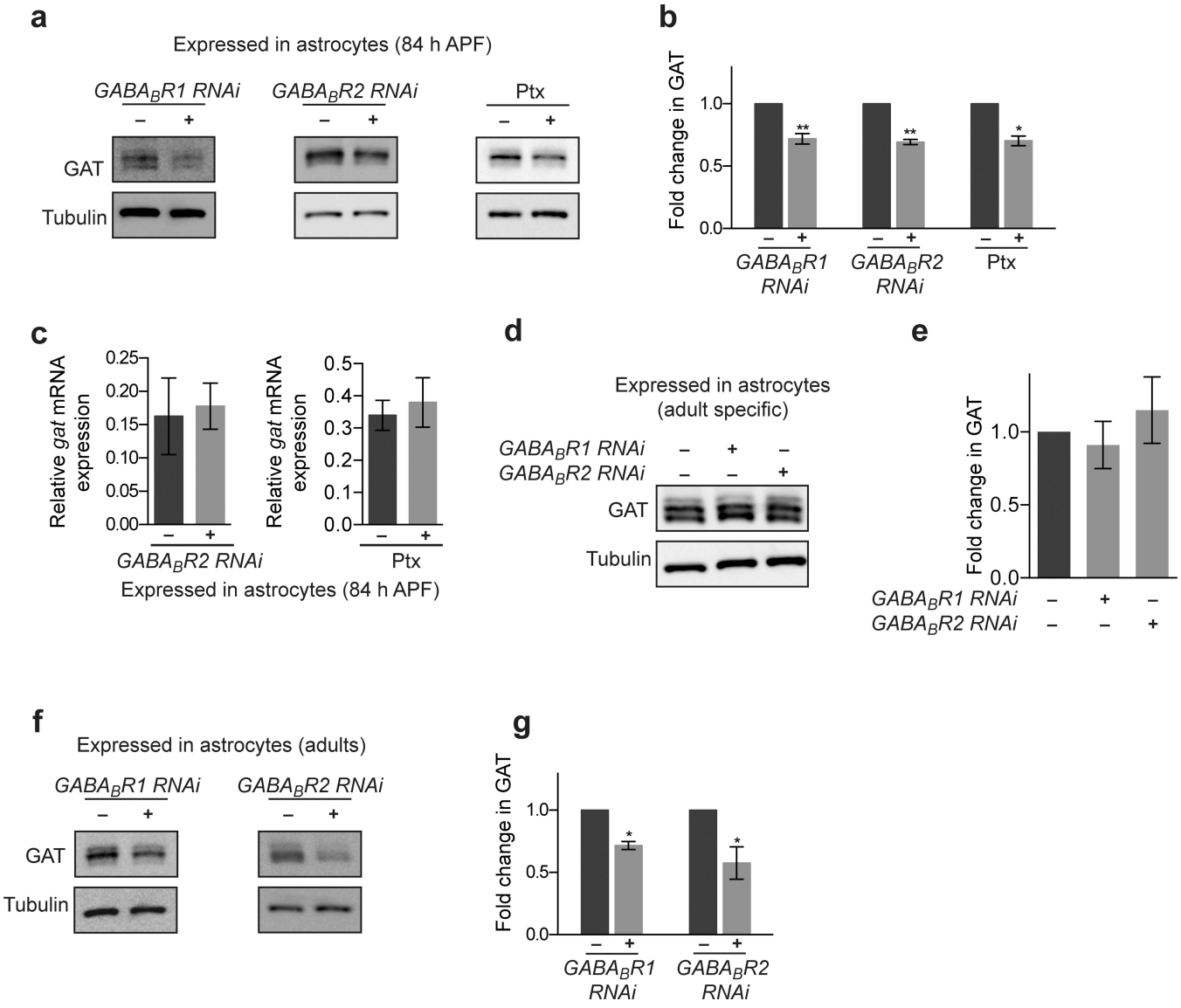


**Figure 7. GAT expression is modulated through astrocytic metabotropic GABA receptors**

**(a)** Western blots performed on brains 84 h APF following inhibition of $GABA_BR1/2$ signaling in astrocytes using the *alrm-GAL4* driver. Blots were probed with anti-GAT antibody. $GABA_BR1/2$ signaling was impaired by expressing *UAS-GABA$_B$R1 RNAi UAS-GABA$_B$R2 RNAi*, or *UAS-ptx*. **(b)** Quantification of GAT levels from Western blot analysis shown in (a) (n = 5 experiments, $GABA_BR1$ RNAi; n = 3 experiments, $GABA_BR2$ RNAi; n = 3 experiments, ptx). **(c)** Relative *gat* mRNA levels are unaltered when astrocytic $GABA_BR1/2$ signaling is perturbed by expressing *UAS-GABA$_B$R2 RNAi* (n = 3 experiments) or *UAS-ptx* (n = 3 experiments) using the *alrm-GAL4* driver. **(d)** Western blots performed on adult brains following adult specific inhibition of $GABA_BR1/2$ signaling in astrocytes. Blots were probed with anti-GAT antibody. **(e)** Quantification of GAT levels from Western blot analysis shown in (d) (n = 3 experiments). **(f)** Western blots performed on adult brains following inhibition of $GABA_BR1/2$ signaling throughout development in astrocytes using the *alrm-GAL4* driver. Blots were probed with anti-GAT antibody. $GABA_BR1/2$ signaling

was impaired by expressing *UAS-GABA$_B$R1 RNAi* or *UAS-GABA$_B$R2 RNAi* though out development. **(g)** Quantification of GAT levels from Western blot analysis shown in (f) (n = 3 experiments, GABA$_B$R1 RNAi; n = 4 experiments, GABA$_B$R2 RNAi). *P≤0.05, **P≤0.01, paired Student's t-test for (b), and (g), unpaired Student's t-test for (c), and 1-way ANOVA with Tukey's post hoc test for (e). Error bars, s.e.m. Full-length blots are presented in Supplementary Fig. 12.

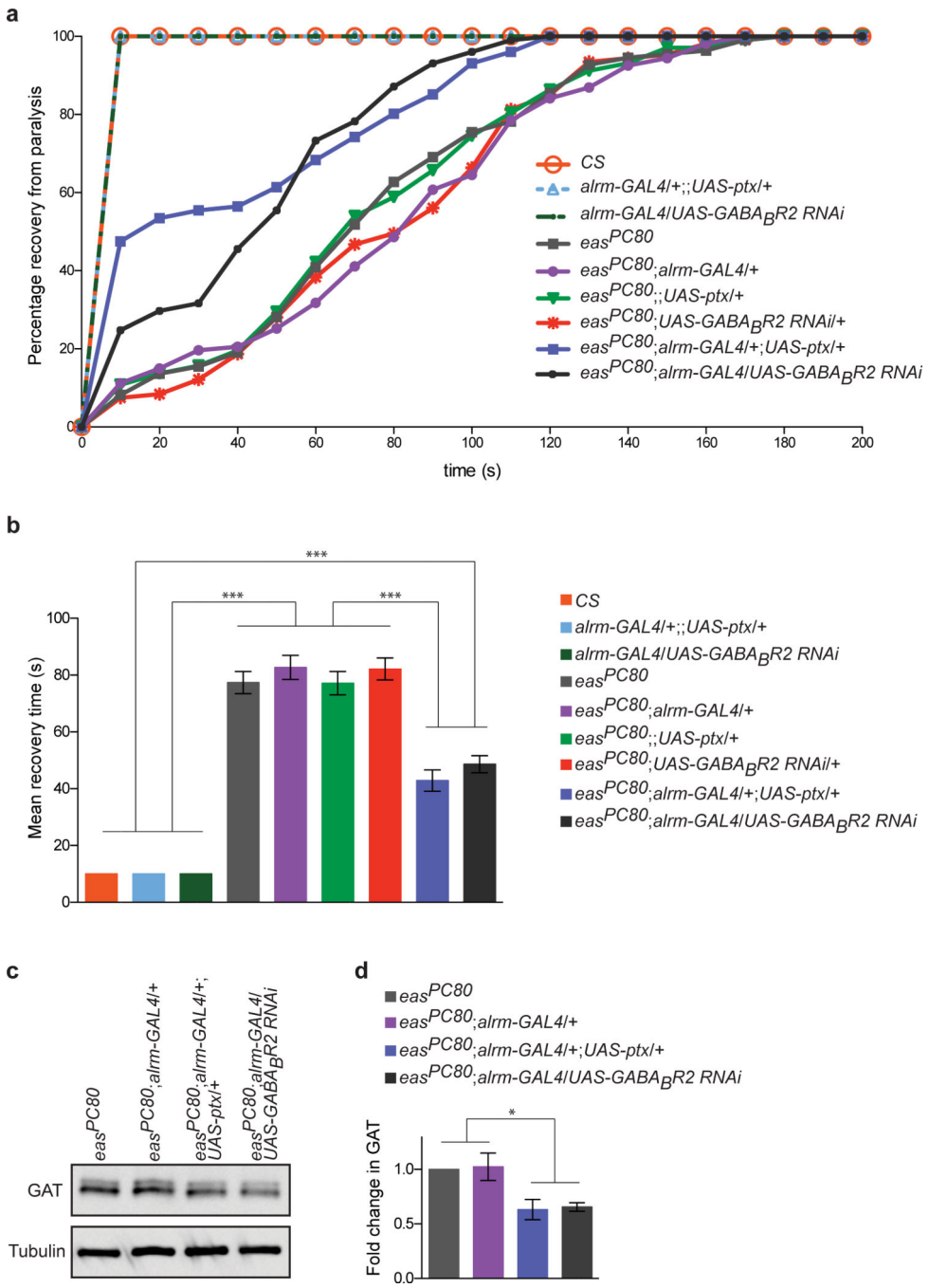


**Figure 8. Regulation of GAT through astrocytic metabotropic GABA receptors can modulate neurotransmission**

**(a)** Flies were vortexed for 10 seconds to provide mechanical stimulation ("bang") and induce paralysis in bang sensitive mutants. The percent of flies recovering from paralysis is shown as a function of time. Flies without the *eas*$^{PC80}$ mutation do not display a bang sensitive phenotype, and therefore 100% of these flies display normal behavior within the first 10 s. *eas* $^{PC80}$ flies and *eas* $^{PC80}$ flies carrying only the *alrm-GAL4* driver or *UAS* constructs display similar recovery response profiles to each other. GABA$_B$R2 signaling was

inhibited in *eas* $^{PC80}$ flies by expressing *UAS-ptx* or *UAS-GABA$_B$R2 RNAi* using the *alrm-GAL4* driver. Recovery profiles are shifted toward shorter recovery times when GAT levels are reduced via inhibition of astrocytic GABA$_B$R1/2 signaling in *eas* $^{PC80}$ flies (n > 100 flies for each genotype). **(b)** Mean recovery time calculated from data shown in (a). **(c)** Western blot performed on adult brain lysates was probed with anti-GAT antibody. In comparison to *eas* $^{PC80}$ flies or *eas* $^{PC80}$ flies carrying the *alrm-GAL4* driver, GAT expression was reduced in *eas* $^{PC80}$ flies expressing *UAS-ptx* or *UAS-GABA$_B$R2 RNAi* using the *alrm-GAL4* driver. **(d)** Quantification of GAT levels from western blot analysis shown in (c) (n = 3 experiments). ***P≤0.001, 1-way ANOVA with Tukey's post hoc test for (b) and repeated measures ANOVA with Tukey's post hoc test for (c). Error bars, s.e.m. Full-length blots are presented in Supplementary Fig. 12.